© Copyright 2020

Miles Freeman

KDM4D Overexpression Enhances Cardiac Regeneration and Mitigates Myocardial Damage in Response to Ischemic Injury

Miles Freeman

A dissertation

submitted in partial fulfillment of the

requirements for the degree of

Doctor of Philosophy

University of Washington

2020

Reading Committee:

W. Robb MacLellan, Chair

Hannele Ruohola-Baker

Michael Regnier

Program Authorized to Offer Degree:

Molecular and Cellular Biology

University of Washington

Abstract

KDM4D Overexpression Enhances Cardiac Regeneration And Mitigates Myocardial Damage In Response To Ischemic Injury

Miles Freeman

Chair of the Supervisory Committee:
Professor W. Robb MacLellan
Department of Cardiology

Protection of myocardium as a means to retain cardiac muscle after injury and prevent the development of heart failure has eluded the field for decades. We recently reported that lysine demethylase KDM4D could partially prevent and reverse cell cycle gene silencing, resulting in modest adult cardiac myocyte proliferation. In this study, we examined the role of KDM4D in response to myocardial infarction in the clinically relevant setting of adult mice by inducing overexpression of KDM4D coincident with MI. KDM4D improved cardiac function after MI, however not through proliferation. The primary benefit of KDM4D was the preservation of myocardium through reduced apoptosis. Gene expression and western blot analysis demonstrated an increase in several anti-apoptotic factors. Our findings suggest that KDM4D may potentiate a survival response and mitigate myocardial damage in response to ischemic injury, making it an attractive candidate for future therapeutic development.

TABLE OF CONTENTS

List of Figures iii

List of Tables iv

Chapter 1. Introduction 1

1.1 Regenerative capacity of the mammalian heart 1

1.2 Cardiac myocyte cell cycle 3

1.3 Epigenetic regulation of cell cycle 3

1.4 Figures 6

1.4 Bibliography 8

Chapter 2. KDM4D Improves Response To Myocardial Ischemic Injury 10

2.1 Introduction 12

2.2 Results 14

2.2.1 KDM4D extends the postnatal regenerative window 14

2.2.2 KDM4D induction potentiates ACM cell cycle gene expression 15

2.2.3 KDM4D induction improves cardiac function and reduces scar size post-MI 17

2.2.4 KDM4D induction mitigates acute myocardial injury 48hrs post-MI 18

2.3 Discussion 19

2.4 Methods 23

2.5 Figures 30

2.6 Table 46

2.7 Bibliography 47

Chapter 3. Cardiomyocyte Dedifferentiation and Proliferation via Partial Reprogramming 55

3.1 Introduction 57

3.2 Results 59

3.2.1 ACM-specific 4F reprogramming factor inducible mouse model 59

3.2.2 ACM-specific 4F reprogramming factor constitutively active mouse model 60

3.3 Discussion 62

3.4 Methods 64

3.5 Figures 66

3.6 Table 75

3.7 Bibliography 76

LIST OF FIGURES

Figure 1.1 Cell cycle genes downregulated in cardiac development.. 6
Figure 1.2 Schematic of stable epigenetic silencing of gene expression in CMs... 7
Figure 2.1 KDM4D extends the neonatal regenerative window..... 31
Figure 2.2 KDM4D potentiates CM proliferation in response to MI at P7 33
Figure 2.3 Characterization of KDM4D induction in ACMs 35
Figure 2.4 KDM4D induction reduces infarct scar size 14 days post-MI 37
Figure 2.5 KDM4D induction mitigates acute myocardial injury 48hrs post-MI 39
Figure S2.1 P1 mice display reduced scar and increased CM cell cycling after MI 41
Figure S2.2 iKDM4D mouse model construction and induction protocol 43
Figure S2.3 iKDM4D MI protocol 45
Figure 3.1 Schematic of Yamanaka transcription factors and their role in reprogramming differentiated cells into iPSCs..... 66
Figure 3.2 Schematic of ACM dedifferentiation, proliferation and redifferentiation..... 66
Figure 3.3 i4F mouse model construction and induction protocol 68
Figure 3.4 Characterization of 4F induction in ACMs 70
Figure 3.5 Constitutive 4F mouse model construction and induction protocol..... 72
Figure 3.6 Characterization of constitutive 4F mice..... 74

LIST OF TABLES

Table 2.1 Cardiac function and morphology in KDM4D MI-operated mice 46
Table 3.1 Cardiac function and morphology in 4F MI-operated mice 76

ACKNOWLEDGEMENTS

I want to thank Dr. Robb MacLellan for his mentorship and guidance both in and out of the lab. Dr. MacLellan's encouragement and support have been profoundly impactful, and much appreciated as I progressed through this project. I am also grateful to Dr. Mary Claire-King for her vision and dedication to the creation of the Morehouse School of Medicine-University of Washington Allied Medical Scientist Training Program. My time in this program has been invaluable, allowing me to address challenging research questions with the guidance of an experienced advisory committee devoted to the advancement and development of the next generation of scientists.

Chapter 1. INTRODUCTION

1.1 REGENERATIVE CAPACITY OF THE MAMMALIAN HEART

In the United States alone, cardiovascular disease accounts for roughly a fourth of all deaths, totaling about 650,000 individuals[1]. Disruption of any element of the heart - myocardium, valves, conduction system, and coronary vasculature - can adversely affect pumping efficiency, thus leading to morbidity and mortality. The high morbidity associated with heart disease can be attributed to the adult heart's limited capacity to heal itself after an injury. After an MI, the damaged myocardium becomes replaced by fibrotic scar tissue owing to the minimal regenerative capacity of cardiomyocytes (CMs) in the adult human heart. The presence of scar tissue in the heart results in a loss of pump function and circulatory deficiency. Consequently, the damaged heart follows a remodeling process that results in further fibrosis, loss of myocardium, cardiac dysfunction, and dilatation, ultimately leading to heart failure and death[2]. In the 90's, early attempts of heart regeneration were unable to promote CM renewal with endogenous cells. However, over the last decade, the field has shifted toward stem cells and cardiac cell therapy. Advancement in our understanding of heart regeneration, CM proliferative potential, and epigenetic regulation of gene expression now allows us to build on earlier approaches of cardiac regeneration.

CMs are in a terminally differentiated state, losing their ability to proliferate soon after birth, at which point heart growth becomes predominantly hypertrophic (enlargement of cell size). CM renewal occurs throughout life in mammalian hearts, but at a markedly low rate, estimates range from 0.5% - 1% per year[3]. Genetic tracking studies of non-radioactive stable nitrogen isotope 15N-labeled DNA in mice, determined the origin of new CMs. They showed

that CMs have a renewal rate of 0.8% per year in adult mice, and most of these new CMs are generated from pre-existing CMs rather than from progenitor cells. These studies have bolstered the notion that the adult mammalian heart has no regeneration potential to compensate for lost CMs after injury.

Unlike mammals, lower vertebrates, such as amphibia or fish, can effectively regenerate their hearts, as well as other organs and limbs. In 2002, the ability of the zebrafish heart to regenerate was demonstrated. The Poss group reported full regeneration of the zebrafish heart following the surgical amputation of approximately 20% of the ventricle[5]. Genetic lineage-tracing showed that regenerated zebrafish CMs also originate from the proliferation of pre-existing CMs, not endogenous progenitor or stem cells[6].

Neonatal mice also demonstrate a regenerative capacity for seven days after birth. A study in 2011 demonstrated heart regeneration in neonatal mice after MI[7]. After amputating 15% of their hearts, neonatal mice were able to regenerate their lost myocardium within three weeks. Again, lineage tracing showed that similar to zebrafish, the proliferation of pre-existing CMs was the source of new CMs that replenished the heart, not cardiac progenitors or stem cells. However, the ability to regenerate is lost after postnatal day seven, and subsequent injury cannot be repaired, resulting in fibrotic scarring similar to that seen in humans post-MI.

With a proliferate rate of less than 1% per year, the adult human heart's capacity to regenerate is undoubtedly not enough to compensate for lost myocardium after an infarction. However, minimal CM proliferation at the border of infarct zones has been recently demonstrated adults[4]. Therefore, reactivating CMs proliferative potential may be a possible strategy for restoring function in the injured heart.

1.2 CARDIAC MYOCYTE CELL CYCLE

The neonatal heart grows in size during development by the proliferation of CMs. However, it shifts to mainly hypertrophic growth, losing proliferation potential within a week of birth. CMs undergo a process called terminal differentiation, which is associated with permanent cell cycle exit[8,9,10]. Two events characterize terminal differentiation in ACMs: the upregulation of cardiac-specific adult genes and the stable silencing of late-phase cell cycle genes[8]. The inability of ACMs to proliferate is due to E2F-dependent cell cycle genes downregulating throughout cardiac development. In fact, our lab has shown that, while genes involved in all phases of the cell cycle downregulate. In adult CMs, G2/M and cytokinesis genes are particularly silenced compared to earlier time points in development (**Figure 1.1**). Additionally, studies suggest that epigenetic mechanisms mediate this process of terminal differentiation in ACMs[11].

1.3 EPIGENETIC REGULATION OF CELL CYCLE

Epigenetics can be defined as the regulatory mechanisms of somatically acquired chromatin modifications able to alter gene expression without changing the DNA sequence[12]. Epigenetic mechanisms can act to induce, flexible, short-term gene silencing through histone tail modifications. Or produce more stable, long-term gene expression through DNA methylation[12]. This epigenome control relies on a large number of histone-modifying complexes, DNA methylation enzymes, and non-coding RNAs, which, to a different extent, regulate chromatin structure[13].

Histones can be modified at many sites, principally acetylated, phosphorylated, or methylated[13]. Modified histone residues form the docking site for various chromatin-binding

proteins, which direct the shift between transcriptionally active (euchromatin) and transcriptionally silent (heterochromatin) chromatin. The reversible nature of histone modifications is attributable to the presence of chromatin remodeling enzymes, with opposing functions. These enzymes (i.e., histone methyltransferases, and their counterpart, histone demethylases) provide for the dynamic structure of chromatin.

Euchromatin is associated with active transcribing genes because its open structure is accessible to transcription factors. In contrast, heterochromatin is a highly dense structure that prevents transcriptional machinery access and gene expression[14]. Histone acetylation is typically associated with euchromatin; on the other hand, histone methylation marks heterochromatin. The effect of histone methylation is dependent on which amino acid residue of the histone is methylated, and whether the residue is mono, di, or trimethylated (me1, me2, and me3, respectively). For example, methylation of the lysine 4, 36, or 79 lysine residue of histone 3 (H3K4me, H3K36me, and H3K79me) at gene promoters denotes transcriptional activation. However, methylation of the 9^{th} or 27^{th} lysine's (H3K9me, H3K27me) is essential to heterochromatin formation and gene repression[15].

At the molecular level, the nuclei of ACMs demonstrate the accumulation of heterochromatin, a characteristic feature of the irreversible cell cycle exit seen in terminally differentiated cells[16]. These heterochromatic regions are characterized by histone hypoacetylation and enrichment of H3K9me3. As CMs develop from proliferating fetal CMs to terminally differentiated adult CMs, the epigenetic landscape changes dramatically. Going from a state of hyperacetylation to a state of hypoacetylation with H3k9me3 enrichment of histones[11](**Figure 1.2**).

Prior to the discovery of histone demethylases[17], H3K9me3, and histone methylation, in general, was considered to be a stable mark[18]. However, the fluid nature of histone methylation is continuing to be uncovered, though little is known about the functions of histone demethylases in the heart. Intriguingly, members of the KDM4 family of H3K9me3 demethylases, are upregulated in some forms of cancer and are believed to promote cellular proliferation and survival[19]. However, these demethylases are downregulated in terminally differentiated ACMs. One KDM4 family member, KDM4D, has a robust and specific H3K9-demethylase activity[20], making it particularly useful as an experimental tool to study the significance of H3K9me3 in regulating cardiac growth and gene expression.

1.4 FIGURES

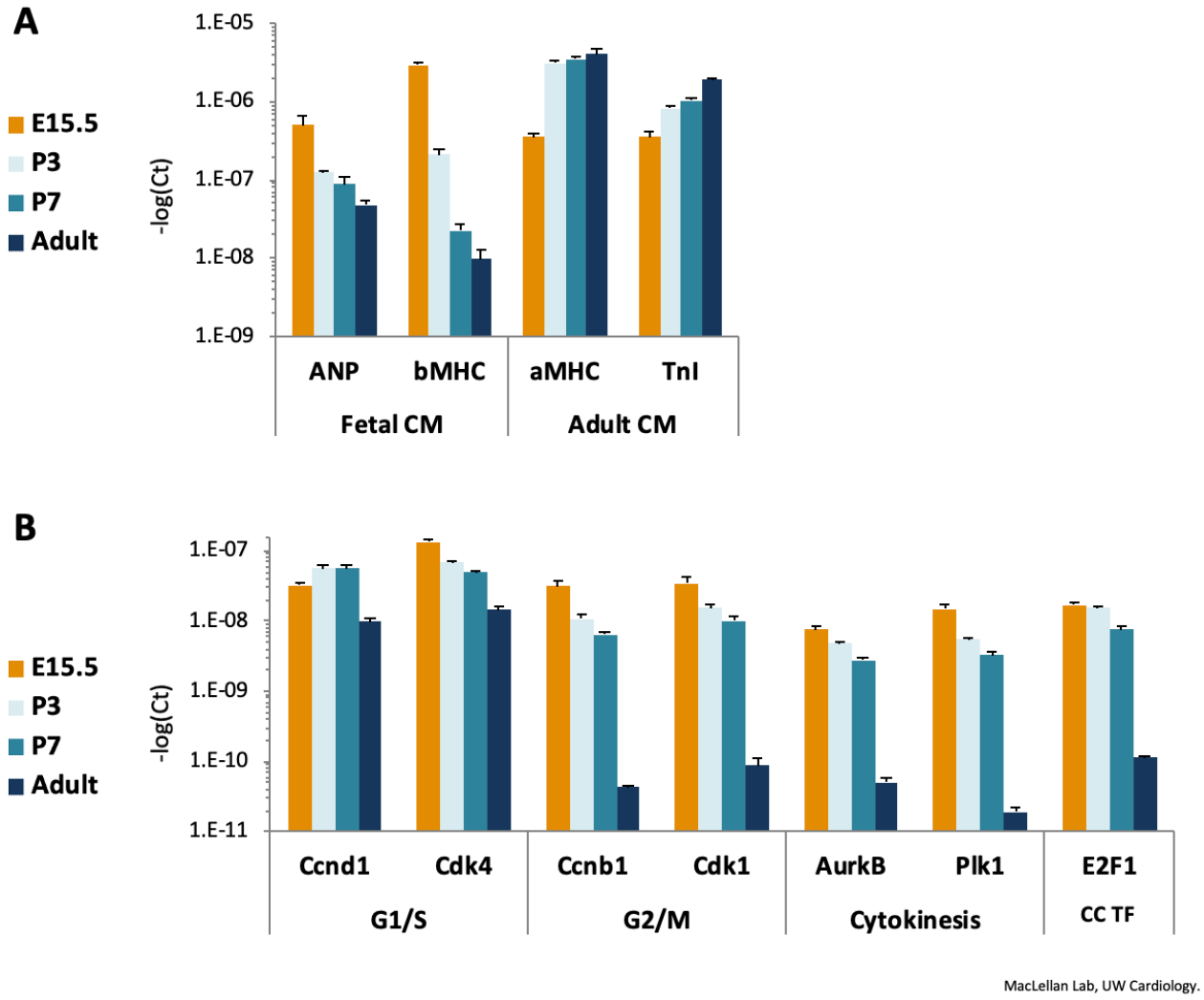

Figure 1.1: Cell cycle genes are downregulated in cardiac development. The loss of proliferative capacity in ACMs correlates with the upregulation of cardiac-specific adult genes and stable silencing of late-phase cell cycle genes. (A) Gene expression analysis studies conducted through CM development reveals the upregulation of αMHC and TnI, cardiac-specific adult genes, from E15.5 to adult. (B) Downregulation in adult CMs of late cell cycle G2/M and cytokinesis genes.

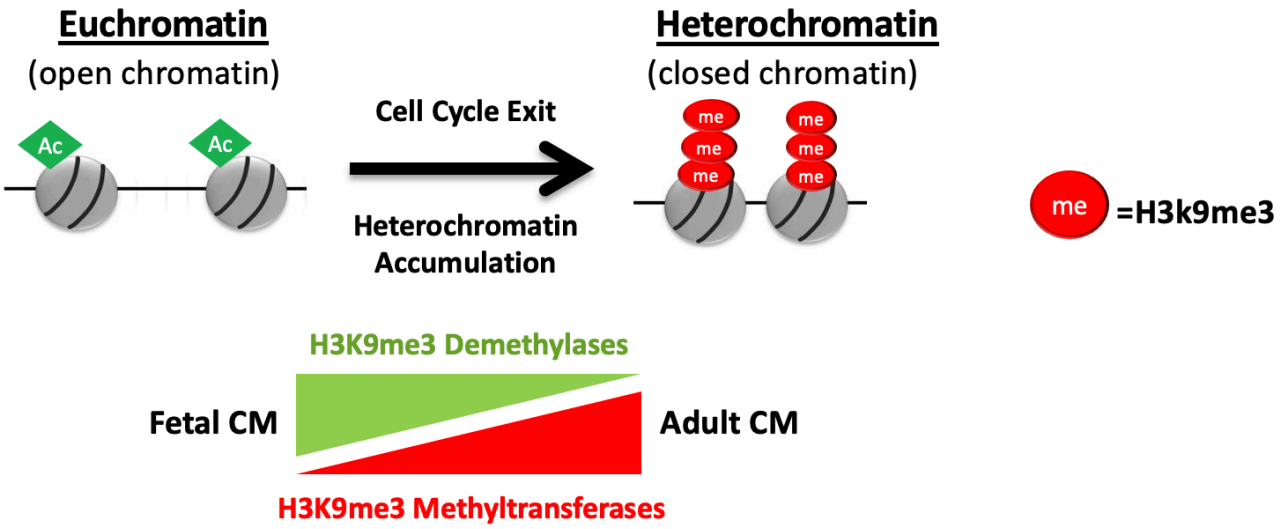

Figure 1.2: Schematic of stable epigenetic silencing of gene expression in CMs. During CC exit, heterochromatin accumulates in the nuclei of terminally differentiated cells. As CMs develop from proliferating fetal CMs to terminally differentiated adult CMs, the epigenetic landscape changes dramatically. Increased levels of H3K9me3 methyltransferases and reductions in H3K9me3 demethylases, lead to the enrichment of H3K9me3 and formation of heterochromatin in ACMs.

1.5 BIBLIOGRAPHY - CHAPTER 1

1. Benjamin EJ, Muntner P, Alonso A, Bittencourt MS, Callaway CW, Carson AP, et al. Heart disease and stroke statistics—2019 update: a report from the American Heart Association. *Circulation*. 2019;139(10): e56–528.
2. Cohn JN, Ferrari R & Sharpe N Cardiac remodeling — concepts and clinical implications: a consensus paper from an international forum on cardiac remodeling. *J. Am. Coll. Cardiol*. 35, 569–582 (2000).
3. Laflamme MA, Murry CE. *Nature* 2011; 473:326-335.
4. Senyo SE, Steinhauser ML, Pizzimenti CL, et al. Nature 2013; 493:433-436.
5. Poss KD, Wilson LG, Keating MT. Heart regeneration in zebrafish. Science. 2002;298(5601):2188–2190.
6. Jopling C, Sleep E, Raya M, *et al. Nature* 2010; 464:606-609.
7. Porrello ER, Mahmoud AI, Simpson E, et al. Science 2011; 331:1078-1080.
8. Ahuja, Preeti et al. “Cardiac myocyte cell cycle control in development, disease, and regeneration.” Physiological reviews vol. 87,2 (2007): 521-44.
9. Mollova, Mariya et al. “Cardiomyocyte proliferation contributes to heart growth in young humans.” Proceedings of the National Academy of Sciences of the United States of America vol. 110,4 (2013): 1446-51.
10. Naqvi, Nawazish et al. “A proliferative burst during preadolescence establishes the final cardiomyocyte number.” Cell vol. 157,4 (2014): 795-807.
11. Sdek P., Zhao P., Wang Y., Huang C. J., Ko C. Y., Butler P. C., et al. (2011). Rb and p130 control cell cycle gene silencing to maintain the postmitotic phenotype in cardiac myocytes. *J. Cell Biol.* 194 407–423

12. Berger, S.L.; Kouzarides, T.; Shiekhattar, R.; Shilatifard, A. An operational definition of. epigenetics. *Genes Dev.* 2009, *23*, 781–783.

13. Illi, B.; Colussi, C.; Grasselli, A.; Farsetti, A.; Capogrossi, M.C.; Gaetano, C. NO sparks off chromatin: Tales of a multifaceted epigenetic regulator. *Pharmacol. Ther.* 2009, *123*, 344–352.

14. Johnson A., Wu R., Peetz M., Gygi S. P., Moazed D. (2013). Heterochromatic gene silencing by activator interference and a transcription elongation barrier. *J. Biol. Chem.*288 28771–28782

15. Chen T., Dent S. Y. (2014). Chromatin modifiers and remodelers: regulators of cellular differentiation. *Nat. Rev. Genet.* 15 93–106

16. Narita M., Nunez S., Heard E., Narita M., Lin A. W., Hearn S. A., et al. (2003). Rb-mediated heterochromatin formation and silencing of E2F target genes during cellular senescence. *Cell* 113 703–716

17. Whetstine JR, Nottke A, Lan F et al. Reversal of histone lysine trimethylation by the JMJD2 family of histone demethylases. *Cell* 2006 May 5;125(3):467-81.

18. Bannister AJ, Kouzarides T. Reversing histone methylation. *Nature* 2005 August 25;436(7054):1103-6.

19. Berry WL, Janknecht R. KDM4/JMJD2 histone demethylases: epigenetic regulators in cancer cells. *Cancer Res* 2013 May 15;73(10):2936-42.

20. Krishnan S, Trievel RC. Structural and functional analysis of JMJD2D reveals molecular basis for site-specific demethylation among JMJD2 demethylases. *Structure* 2013 January 8;21(1):98-108.

Chapter 2. KDM4D IMPROVES RESPONSE TO ISCHEMIC MYOCARDIAL INJURY

A version of this chapter is currently in preparation for submission for publication as:

KDM4D Overexpression Enhances Cardiac Regeneration And Mitigates Myocardial Damage In Response To Ischemic Injury
Miles Freeman, Danny El-Nachef, Hidemi Kajimoto, Allison Williams, Zhanhe Zhang, George Davenport, Yiqiang Zhang, W. Robb MacLellan

ABSTRACT

In mammals, fetal cardiac myocytes proliferate robustly but lose this ability within a week after birth through the downregulation of cell cycle genes. Adult cardiac myocytes (ACMs) show very limited capacity to proliferate so developing therapeutic strategies that promote proliferation or survival of endogenous cardiac myocytes after an injury is of great interest. We have shown that overexpression of the lysine demethylase KDM4D could prevent or reverse cell cycle gene silencing, resulting in modest ACM proliferation. In this study, we examined the role of KDM4D in the regenerative response to myocardial infarction (MI). Overexpression of KDM4D in neonatal hearts after their withdrawal from cell cycle reduced scarring from ischemic injury by increasing re-expression of cell cycle genes and stimulating myocardial proliferation. Inducing KDM4D in adult myocardium coincident with MI led to a reduction in left ventricular scarring and improved function. While KDM4D enhanced ACM cycling, a novel benefit the preservation of myocardium through reduced apoptosis. KDM4D activated the expression of several anti-apoptotic factors, including Bcl2, APAK, and survivin. These results suggest that KDM4D may also mitigate myocardial damage in response to ischemic injury, making it an attractive candidate for future therapeutic development.

2.1 INTRODUCTION

The limited potential of adult mammalian hearts to regenerate lost myocardium after an injury is a significant factor in the progression to heart failure[1]. Although new cardiac myocytes (CM) are generated in adult hearts, it is insufficient for the restoration of contractile dysfunction after myocardial infarction (MI)[2–4]. Increasing evidence suggests that the limited new CMs that are formed arise from the proliferation of pre-existing CMs[4,5]. The lack of regeneration in adult murine hearts contrasts with the substantial cardiac regeneration seen in newborn mice[6–8]. Genetic fate-mapping studies in these neonatal hearts revealed that the new CMs in this regenerative response also came from the proliferation of pre-existing CMs[6,7]. However, the regenerative capacity seen in newborn mice is lost by postnatal day 7 (P7), and subsequent injury leads to fibrotic scarring similar to what follows after injury in adult hearts[6–10]. The decline in regenerative capacity by P7, and in adult CMs is a process called terminal differentiation, characterized by permanent cell cycle arrest. Thus, efforts to develop therapeutic interventions in response to injury in adult hearts have focused on strategies that either salvage myocardium or restore the proliferative capacity of ACMs to promote adult heart regeneration.

The molecular basis for the limited capacity of ACMs to proliferate is poorly understood, but when subjected to a growth stimulus, they preferentially undergo an increase in cell size (hypertrophy) rather than dividing[11]. Interestingly, despite the lack of division, stimulating mitogenic pathways in ACMs can lead to the induction of G1/S phase genes, DNA synthesis, and increases in DNA content[4,12–15]. However, G2/M and cytokinesis genes remain silenced[14]. This inability to up-regulate late cell cycle genes is consistent with ACMs being unable to complete the later phases of the cell cycle. The stable silencing of gene expression is controlled by epigenetics, which regulates gene activity through remodeling of chromatin structure[16].

Epigenetic regulation involves modifications of either DNA (DNA methylation) or through the post-translational modification of histones, including acetylation and methylation[17]. These modifications, at least methylations, were long assumed to be stable; however, the recent identification of histone modification enzymes suggests that epigenetic regulation can be dynamic and reversible[18]. One methylation commonly associated with transcriptionally silent is the trimethylation of lysine 9 on histone H3 or H3K9me3.

To understand the role of H3K9me3 in ACMs, we created a transgenic mouse model where H3K9me3 was specifically depleted in CM using lysine demethylase 4D (KDM4D), a member of the histone demethylase family of enzymes. Constitutive, CM-specific expression resulted in a delay in CM cell cycle exit and increased ACM expression of G2/M and cytokinesis genes *in vivo*[19]. Although highly upregulated compared to controls, late cell cycle gene expression in KDM4D expressing ACMs was still much less than in wildtype fetal CMs[19]. Also, the absolute number of cycling CMs, while increased in KDM4D hearts, was low, and normalized cardiac mass did not increase further beyond 9 weeks of age[19].

In this study, we sought to determine whether KDM4D expressing ACMs are permanently arrested or could potentially proliferate after injury. We tested this hypothesis by subjecting both neonatal and adult KDM4D expressing hearts to ischemic injury via myocardial infarction (MI). KDM4D overexpression enhances the proliferative response after acute MI in neonates but results in only limited CM proliferation in adults. However, in adult mice, it reduced acute myocardial injury. KDM4D upregulation induced expression of genes that regulate damage response and apoptosis pathways, improving myocardial function post-MI. Our *in vivo* study is the first to suggest that KDM4D can regulate not only cell cycling and cellular proliferation but also has a role in controlling ACM's response to injury[20-24].

2.2 RESULTS

2.2.1 *KDM4D extends the postnatal regenerative window.*

To determine whether delaying CM cell cycle exit via KDM4D expression could extend the postnatal regenerative window, we performed MIs at P1 and P7 in control and cardiac-specific KDM4D expressing mice ($KDM4D^{Tg/+}$). The regenerative response at P1 is associated with robust induction of CM proliferation in wild type mice resulting in minimal scarring. In contrast, the proliferative response is lost by P7 leading to substantial replacement fibrosis and scarring (**Figure S2.1A-E**). To evaluate if the lack of proliferation post-MI at P7 is secondary to an inability to induce the necessary cell cycle factors as is seen in adult hearts, we examined cell cycle gene expression in CMs seven days after MIs performed at P1 or P7 (**Figure S2.1F**). All cell cycle genes showed reduced expression in the groups receiving surgeries at P7 versus P1. In Sham mice, the expression levels of Ccnb1, Plk1, and Aurkb were 2.4 to 3.3-fold higher in the P1-sham group compared to the P7-sham group ($P<0.05$). Notably, in animals receiving either surgery at P1, cell cycle genes were highly expressed seven days later in P8 CMs, with MI further increasing only the expression levels of Plk1. There was no significant induction of cell cycle genes by MI at P7.

To establish if removing the potentially negative regulator, H3K9me3 could restore cell cycle gene expression and neonatal CM cycling after MI at P7; we utilized CM-specific KDM4D-overexpressing mice[19]. We confirmed that KDM4D induction depleted H3K9me3 in postnatal $KDM4D^{Tg/+}$ CMs (**Figure 2.1A**), and we initially assessed whether the acute injury was similar after ischemic injury between P7-$KDM4D^{Tg/+}$ and littermate control mice. There was no difference in acute injury response to ischemia (**Figure 2.1B**). However, at 21 days post-MI, control hearts displayed fibrotic scar (% average scar/LV area was $12.8\pm3.4\%$, and the

maximum % scar/LV area was 18.8±3.6%, **Figure 2.1C-2.1E**). We also observed ventricular dilation consistent with no regeneration (**Figure 2.1E**). In contrast, KDM4D$^{Tg/+}$ hearts showed minimal scarring with a predominance of normal-appearing myocardial tissue (% average scar/LV area was 4.2±1.5%, and the maximum % scar/LV area was 8.3±2.1%, $P<0.05$ vs. control hearts; **Figure 2.1C-2.1E**).

To verify if the regeneration seen after P7 MI in KDM4D hearts was related to enhanced CM proliferation, we analyzed CM cycling with a panel of cell cycle markers. In control hearts, BrdU-positive cells were mainly seen in non-CMs 21 days after MI (**Figure 2.2A**). In contrast, cycling CMs were detected in KDM4D$^{Tg/+}$ hearts after MI, with BrdU-positive CMs representing ~15% of KDM4D$^{Tg/+}$ CMs in both border and remote zones (**Figure 2.2A**). While MI at P7 did not increase pH3 positive CMs in control hearts, pH3-positive CMs were upregulated >3-fold after MI in KDM4D$^{Tg/+}$ hearts (**Figure 2.2B**). Analysis of the CM area demonstrated there was no difference in CM size between control and KDM4D$^{Tg/+}$ after sham surgery (**Figure 2.2C**). CM hypertrophy was observed in control animal's post-MI; however, there was no change in CM size in KDM4D$^{Tg/+}$ hearts (**Figure 2.2C**). Late cell cycle gene expression was increased in KDM4D$^{Tg/+}$ CMs compared to control CM after MI (**Figure 2.2D**). G2/M genes (Cdk1 and Ccnb1) and cytokinesis genes (Plk1 and Aurkb) were increased post-MI in KDM4D$^{Tg/+}$ CMs (**Figure 2.2D**).

2.2.2 *KDM4D induction potentiates ACM cell cycle gene expression.*

Since we had previously determined KDM4D could potentiate ACM proliferation at both neonatal time points as well as in adults[19], we decided to test the effect of KDM4D expression on adult ACM proliferation in response to ischemic injury. To address the limitations of our previous studies, which used a transgenic line constitutively active throughout development, we

generated a CM-specific reverse tetracycline transgenic activator line by mating selected reverse tetracycline transactivator[25] (rtTA) and KDM4D tet-responder (tet) lines. This breeding produced inducible KDM4D animals (iKDM4D) that displayed a tightly regulated KDM4D gene expression in the heart upon doxycycline treatment (**Figure S2.2A**). This enabled assessment of whether KDM4D could reverse the ACM cell cycle exit after CMs underwent normal terminal differentiation, which is more applicable to clinical applications. Induction of KDM4D and the depletion of H3K9me3 (**Figure 2.3A**), as well as the up-regulation cell cycle genes (**Figure 2.3B**), were confirmed in this model with two weeks of induction using doxycycline chow. The late cell cycle genes *Cdk1* and *AurkB* were up-regulated 4-fold and 6-fold, respectively ($P<0.05$). KDM4D induced no significant difference in HW/BW in iKDM4D mice compared to control mice (**Figure 2.3C**). However, quantification of isolated CMs area determined CMs from iKDM4D hearts had an average area 30% smaller than control CMs, respectively ($3437\mu m^2 \pm 55\mu m^2$; $4993\mu m^2 \pm 350\mu m^2$ $P<0.01$; **Figure 2.3D**).

To identify increases in ACM cell cycling, we administered BrdU weekly for two weeks and quantified the amount of CMs that underwent DNA synthesis. Analysis of iKDM4D versus control hearts demonstrated a 4-fold increase in BrdU positive CM nuclei/mm^2 in iKDM4D compared to control (iKDM4D 2.5 ± 0.3 vs. control 0.6 ± 0.04, $P<0.05$; **Figure 2.3E**). Additionally, the assessment of mitotic stimulation in CM by Ki67 staining showed a significant increase in iKDM4D hearts versus control (iKDM4D 0.3 vs. control 0.1, $P<0.05$; **Figure 2.3F**). Our results demonstrate that H3K9me3 depletion via KDM4D induction leads to an upregulation of late cell cycle genes, as well as an increase in BrdU (DNA synthesis) and Ki67 (mitotic stimulation). Although we do not see a significant difference in HW/BW after a two-week induction we do see a trend of iKDM4D (+Dox) animals with higher average HW/BW of

5.5mg/g compared to controls (-Dox) of 4.9mg/g, suggesting more induction time, may lead to further stratification of HW/BW.

2.2.3 *KDM4D induction improves cardiac function and reduces scar size post-MI.*

To determine if re-expression of KDM4D after CM terminal differentiation would allow CM proliferation and regenerative response in adults, we subjected iKDM4D and control littermates to sham or MI surgeries at 8-10 weeks of age. The mice were started on doxycycline chow to induce KDM4D expression immediately post-op to mimic a more clinically relevant setting (**Figure S2.3A**). Analysis of cardiac function 14-days post-MI showed reduced ejection fraction (EF) and fractional shortening (FS) in control animals as expected. Cardiac function iKDM4D mice was significantly preserved (EF- control 30.2% vs. iKDM4D 50.8%, $P<0.05$; FS- control 13.9% vs. iKDM4D 26.7%, $P<0.05$, **Table 2.1**). Furthermore, scar size was reduced by nearly half in iKDM4D hearts after MI compared to control (3.1% vs. 5.8% fibrosis of the myocardium, $P<0.05$, **Figure 2.4A**).

To determine if this preservation of cardiac function and reduction in fibrotic scarring occurred primarily through ACM hyperplasia, we analyzed a panel of cell cycling markers. There was a 3.7-fold increase in Ccnd1 and a 1.5-fold increase in Cdk1 gene expression compared to control post MI $P<0.05$. However, no further increases in cytokinesis gene expression were observed post MI (**Figure 2.4D**). BrdU incorporation and pH3 staining also confirmed low levels of DNA synthesis and mitotic stimulation in activated iKDM4D hearts relative to controls two weeks post-MI (**Figure 2.4E- 2.4F**). HW/BW and morphological analysis demonstrated that there was no significance in size differences of iKDM4D hearts or ACMs compared to controls post-MI (**Figure 2.4B-2.4C**). Overall, ACM cell cycle activity in

adults after KDM4D induction post-MI revealed less robust CM cell cycling compared to P7-KDM4D$^{Tg/+}$ hearts.

2.2.4 *KDM4D induction mitigates acute myocardial injury 48hrs post-MI.*

Given the less robust CM proliferative response in adults versus neonates, we analyzed whether KDM4D could be preserving myocardium through other mechanisms as well. H3K9me3 can regulate the expression of genes controlling the cellular damage response, so myocardial salvage is an alternate explanation for reduced scarring[20-24]. To determine whether KDM4D was regulating cell death in ACMs, we performed a triphenyl tetrazolium chloride (TTC) assay on iKDM4D and control hearts 48 hours post-MI. In contrast to neonatal hearts, the infarct size was smaller in iKDM4D animals compared to controls (6.1% vs. 10.3% infarct size, $P<0.05$, **Figure 2.5A**). At this time point, no significant cell cycle induction had yet occurred (**Figure 2.5B**). However, several genes involved in cellular apoptosis and survival, including *Bcl-2, Survivin,* and *APAK,* were significantly increased in iKDM4D CMs compared to control, respectively (3-fold, 1.7-fold, and 2.3-fold increase, $P<0.05$. (**Figure 2.5C**). APAK protein was also increased 48 hrs post-MI compared to control (**Figure 2.5D**). To determine if the expression of these factors reduced the apoptosis typically seen post-MI, we quantified apoptosis using the TUNEL assay. iKDM4D hearts showed a 3.4-fold decrease in TUNEL-positive CMs compared to control hearts (iKDM4D 0.06+CM/mm^2 vs. control 0.2+CM/mm^2 $P<0.05$, **Figure 2.5E**).

2.3 DISCUSSION

The finding that mammalian hearts can regenerate after injury in neonates through CM proliferation has reinvigorated attempts to stimulate CM division in adults[26]. The difference in response to MI at P1 versus P7 appears to be related to the persistent expression of cell cycle genes and the ability of cardiac myocytes to proliferate at P1 but not P7. This inability to divide at P7 replicates the response to injury seen in adult hearts[7,9]. Our data demonstrates that CM-specific overexpression of KDM4D and depletion of H3K9me3 extends the neonatal regenerative window allowing CM proliferation even at P7. It also permits limited CM cycling in ACMs. Unexpectedly, we also found a role for H3K9me3 in regulating CM death through the repression of genes responsible for the regulation of distinct cellular damage response processes (**Figure 2.5**).

Transcriptional analysis of cardiomyocytes has shown distinct differences in the inflammatory response of the injured neonatal and adult heart, which potentially triggers a regenerative or fibrotic repair process in the heart[27]. Neonatal CMs retain cell-cycle gene expression, suggesting they exist in a permissive state that allows them to proliferate after injury. Thus, neonatal heart regeneration in mammals may rely on a permissive embryonic developmental state that is retained transiently following birth. Neonatal CM, even at P7, exists in a more permissive embryonic developmental state allowing for stimulation and activation of regenerative pathways. Whereas, ACMs have undergone terminal differentiation and are in a more senescent state, thereby rendering a different response upon injury.

H3K9me3's function in cellular development, acting as a repressor of inappropriate lineage genes, and preserving cell integrity has been demonstrated in numerous studies. Additionally, over recent years several diverse roles for H3K9me3 have been identified,

including regulating apoptosis[20, 28], autophagy[29], development[30], DNA repair[22–24], self-renewal[31], and aging[32], among others. H3K9me3 silences gene expression by interacting with the amino-terminal chromodomain of heterochromatin protein 1 (HP1), recruiting it to specific chromatin loci[33,34]. Through binding with HP1 protein, H3K9me3 recruits additional epigenetic modifications to stabilize the repressive chromatin structure[35]. Rb also interacts with HP1 adapter proteins[36,37], suggesting that removal of H3K9me3 could disrupt the repressive complexes that suppress cell cycle genes in CM. Consistent with this, our lab found that ACM-specific Rb deletion combined with p130 knockout led to increased cell cycle gene expression, but H3K9me3 was maintained[14]. Thus, H3K9me3-depletion may reduce cell cycle gene silencing through Rb and H3K9me3-binding adapter proteins. Although H3K9me3 itself is not specific to cell cycle genes, H3K9me3 depletion could specifically increase cell cycle gene expression through the disruption of specific inhibitory complexes that bind H3K9me3 or H3K9me3-adapter proteins.

The role of apoptosis in ischemic heart disease, particularly myocyte cell death in acute myocardial infarction has been well characterized[38]. The progressive LV remodeling that occurs after MI leading to heart failure is also associated with ongoing apoptosis[39,40]. We found that the depletion of H3K9me3 leads to the upregulation of pro-survival pathways, including Bcl-2, survivin, and APAK, which was associated with reduced apoptosis and smaller infarct size in iKDM4D mice (**Figure 2.5C**). Manipulation of these factors have been shown to promote CM survival in response to ischemia by other investigators. Overexpression of anti-apoptotic Bcl-2 protein or genetic deletion of pro-apoptotic Bax protein prevents apoptosis and reduces infarct size after myocardial infarction[41-44]. Survivin's anti-apoptotic function is related to its ability to interfere with apoptosome complex recruitment and reducing apoptosis via inhibition of caspase-

9 activation[45-47]. It also plays an essential role in cell division[48], recruiting members of the chromosomal passenger complex, including Aurora B[49-51]. Overexpression of survivin both prevented apoptosis and increased CM proliferation after myocardial infarction[47]. KDM4D also induced APAK, a known regulator of p53-mediate apoptosis. p53 is a well-established mediator of CM injury after hypoxia or ischemia[52,53]. Ablation of p53 protects against the development of cardiac dysfunction after ischemic injury[54]. These effects were due to the activation of genes involved in the inhibition of apoptosis[54].

Our data suggest a novel interplay between cell cycle control and cell death in CMs. In contrast, there are well-established links between cell cycle and apoptosis in cancer cells, which are often enriched in genes in both pathways. *p53* acts early in the cell cycle by blocking cell cycle progression in the G1 phase. DNA damage, hypoxia, or oncogenic stimuli, among others, activates *p53*[55] and this activation leads to G1 arrest by inducing the expression of p21, a cyclin-dependent kinase inhibitor. Studies have also associated p53 with the regulation of the G2/M checkpoint[56,57]. Besides regulating the cell cycle, p53 also plays an essential role in triggering apoptosis within cells. Typically, *p53*-induced apoptosis is independent of a transcriptional function. Occurring in the presence of p53 protein synthesis inhibitors[58]. However, *p53* also represses the transcription of specific genes that inhibit its ability to induce apoptosis, such as Bcl-2[59]. APAK, a p53 regulator, has been shown to aid in the control of p53-mediated cell cycle arrest or apoptosis[60,61]. APAK binds directly to p53 in unstressed cells, suppressing p53-mediated apoptosis by recruiting KRAB-box-associated protein and histone deacetylase 1 to reduce the acetylation of p53. APAK represses p53 activity by interacting with ATM, a p53 activator. In response to stress, APAK is phosphorylated by ATM and dissociates from p53, resulting in activation of p53 and induction of cell cycle arrest and apoptosis[62]. Recently,

H3K9me3 was shown to directly regulate APAK, repressing gene expression as H3K9me3 accumulates along the *APAK* loci[20]. H3K9me3 also indirectly represses APAK by stimulating ATM activity[63] through the regulation of Tip60, which acetylates ATM[64]. APAK-induction through H3K9me3 reduction may remove both an essential barrier to cell cycle progression and proliferation while simultaneously reducing a principal driver of apoptosis after injury through the regulation of p53.

We originally sought to better understand the molecular blockades to ACM division that limit CM proliferation. However, we found that H3K9me3 also plays a pivotal role in controlling myocyte death in the adult myocardium. This study demonstrated for the first time that decreasing the levels of H3K9me3, through induction of KDM4D promote ACMs survival after ischemic injury (**Figure 2.5**). Thus, KDM4D holds tremendous promise as a therapeutic tool both through facilitating CM cell cycle progression and mitigating ACM damage from ischemic injury in adult myocardium.

2.4 METHODS

Mouse Studies. All animal studies were performed in accordance with an approved Institutional Animal Care and Use Committee (IACUC protocol #4290-01), the University of Washington institutional guidelines, and the National Institute of Health Guide for the Care and Use of Laboratory Animals. The αMHC-tTA (tet-off) mice used for constitutive CM-specific transgene expression was generated by the Robbins lab[65]. The αMHC-rtTA (tet-on) mice used for inducible ACM-specific transgene expression was generated by the Valencik Lab[25]. Transactivator lines were crossed with the tet-responsive KDM4D mice we previously made[19] to generate the $KDM4D^{Tg/+}$ model. For temporal control of transgene activity we used doxycycline-containing chow (Harlan TD.00502) administered ad lib for the indicated times. Cardiac injury model was created by inducing a MI by LAD occlusion in adult mice (8-10 weeks), as has been previously described[66]. Sham-operated mice underwent the same procedure involving hypothermic anesthesia and thoracotomy without LAD ligation. Littermate controls were used for all experiments involving transgenic mice (n=53).

Assessment of neonatal MI. To assess infarct size, 2,3,5-Triphenyltetrazolium chloride (TTC) staining was performed 3 days after MI. To delineate infarcted from viable myocardium, the hearts were incubated in a 1% solution of triphenyltetrazolium chloride (TTC) in phosphate buffer (pH 7.4) at 37 °C for 5 minutes. The hearts were fixed in 10% neutral buffered formaldehyde at room temperature for 20 minutes and photographed. The percentage of viable (red) and dead (white) myocardium 24 h after MI was quantified by using Adobe Photoshop software (Adobe systems). Fibrotic area was determined 21 days after MI. Serial sections were cut at 200-μm intervals from the site of the ligature toward the apex. Sirius red/fast green

staining was performed. Fibrotic area (%) = (the sum of fibrotic area at L600 and L800 / the sum of myocardial area in the LV at L600 and L800) × 100.

Assessment of adult MI. To assess infarct size, TTC staining was performed 2 days after MI. To delineate infarcted from viable myocardium, the hearts were incubated in a 1% TTC in phosphate buffer (pH 7.4) at 37 °C for 5 minutes. The hearts were fixed in 10% neutral buffered formaldehyde at room temperature for 20 minutes and photographed. The percentage of viable (red) and dead (white) myocardium 48hr after MI was quantified by using Image J software. Fibrotic area was determined 14 days after MI. Serial sections were cut at 200-μm intervals from the site of the ligature toward the apex. Trichrome staining was performed. Infarct scar area and the total area of myocardium were traced manually in Image J and measured automatically by the computer. Infarct size, was expressed as a percentage, and was calculated by dividing the sum of infarct areas from all sections by the sum of LV areas from all sections (including those without infarct scar) and multiplying by 100.

2-D Echocardiography. Under 0.5% isoflurane, mice EKG and heart function were assessed using Visual Sonics Vevo 2100. Parasternal short axis images at the plane of the papillary muscle were collected in B- and M-Modes. Images were collected with heart rates ranging from 400-500 BPMs. Imaging and analysis were performed by a single operator who was blinded to the genotypes. Quantification of images was performed using Vevo Labs 1.7.0, according to the manufacturer's guidelines.

CM cell isolation. We utilized established protocols for CM isolations[14,20]. Briefly, heparinized mice were euthanized with isoflurane and hearts were extracted and arrested in KB buffer (mmol/L: KCl 20, KH_2PO_4 10, K+-glutamate 70, $MgCl_2$ 1, glucose 25, taurine 20, EGTA 0.5, HEPES 10, 0.1% albumin, pH 7.4 with KOH). For purified ACM preparations, the aorta was

cannulated, and the heart was washed with Tyrodes solution (pH 7.4, supplemented with 25uM Blebbistatin -/-) and digested for 7 minutes with collagenase II (Worthington 4176) and Protease Streptomyces griseus XIV (Sigma P5147) using Langendorf perfusion. Ventricles were dissociated and the resulting cell suspension was filtered through a 100μm mesh. Three rounds of low speed centrifugation, where ACMs are loosely pelleted and non-CMs in suspension are aspirated, density purify the ACM population, resulting in >90% rod-shaped ACMs. For embryonic and postnatal CM preparations, hearts were washed in Ads buffer (mmol/L: NaCl 116, HEPES 20, NAH_2PO_4 10.8, glucose 5.5, KCl 5.4, $MgSO_4$ 0.83) and incubated with enzyme solution (Collagenase II, Pancreatin (Sigma P3292)) with rotation. Freed cells were collected into serum (stopping digestion) every 20 minutes, resulting in dissociation of the entire heart within 2 hours. The resulting cell suspension was fractionated using a percoll (Sigma P4937) gradient, and the CM layer and non-CM layer were each collected. Quality and purity of CM preparations were verified by immunostaining, flow cytometry, and RNA expression of cell-type-specific markers.

Immunoblotting. Immunoblotting was done as described previously[14,20]. CMs were lysed and whole cell lysates were separated on 12% gel, transferred onto PVDF membranes and probed with the following antibodies against: human Myc (Hybridoma bank, Iowa city, IA), H3K9Me3 (Diagenode), and H3 (Millipore).

RNA isolation and analysis. RNA was isolated from cells and tissue using TRISOL (Sigma T9424) phenol/chloroform purification, followed by column purification with DNase treatment (Qiagen 74004). cDNA was synthesized as described in the manufacturer's guidelines (Roche 04896866001). qPCR was performed using SYBR green (Life Technologies 4472908) on a real-time PCR machine (ABI 7900HT). Primers were validated by standard PCR with electrophoresis

to confirm specific target band and lack of primer dimers. qPCR dissociation curves were consistent with a single specific product. Ct values were assigned using ABI's SDS 2.4 software with automated thresholding and baselines. The standard curve method or dCt method was used to quantify expression, and expression of each gene was normalized by *GAPDH*. Standard Curves were generated using tissue or cells that highly express the indicated gene, resulting in qPCR efficiencies ranging from 88-97%.

Mouse: *Gapdh* F-CCAATGTGTCCGTCGTGGATCT, R-GTTGAAGTCGCAGGAGACAACC; *ANP* F-AGGATTGGAGCCCAGAGTGGA, R-TGATAGATGAAGGCAGGAAGC; *bMHC* F-GCGACTCAAAAAGAAGGACTTTG R-GGCTTGCTCATCCTCAATCC; *aMHC* F-AGAAGCCCAGCGCTCCCTCA, R-GGGCGTTCTTGGCCTTGCCT; *cTNI* F-GCAGCCCAGAGGAAACCCAACC R-AGCCGCATCGCTGCTCTCATC; *Ccnd1* F-TGCTGCAAATGGAACTGCTTCTGG, R-TACCATGGAGGGTGGGTTGGAAAT; *Ccne1* F-GCTTCGGGTCTGAGTTCCAA, R-GGATGAAGAGCAGGGGTCC; *Cdk4* F-GGGACCTGAAGCCAGAGAAC, R-CCACAGAAGAGAGGCTTCCG; *Ccnb1* F-GCCTCACAAAGCACATGACTG, R-TCGACAACTTCCGTTAGCCT; *Cdk1* F-GGCGAGTTCTTCACAGAGACTTG, R-CCCTATACTCCAGATGTCAACCGG; *AurkB* F-GCACCTGAAACATCCCAACAT, R-GGTCCGACTCTTCTGCAGTT; *Plk1* F-GTATTCCCAAGCACATCAA, R-GTAGCCAGAAGTGAAGAAC; *E2F1* F-TGCCAAGAAGTCCAAGAATCA, R-CTGCTGCTCACTCTCCTG; *E2F4* F-TGTCCTTGGCAGCACTCA, R-TTCACCACTGTCCTTGTTCTCA; *Rb* F-CCTGATAACCTTGAACCTGCTTGT, R-GCTGAGGCTGCTTGTGTCT; *p130* F-CACCGAACTTATGATGGACAG, R-ATGGCTTCTGCTCTCACT; *p107* F-GCAGAGGAGGAGATTGGAACA, R-GCTACAGGCGTGGTGACT; *p21* F-

GCAGACCAGCCTGACAGATTT, R-CTGACCCACAGCAGAAGAGG; *p53* F-CAGTGGGAACCTTCTGGGAC, R-CGCGGATCTTGAGGGTGAAA *KDM4A* F-CTGCTAGGGCTTTAGGCTCC, R-TTTGGGAGGAACGACCTTGG; *KDM4B* F-CAGAGAGCATCACGAGCAGA R-CTCTTGGGCAGCTCCTCTTC; *KDM4C* F-GCGGGTTCATGCAAGTTGTT, R-GTTTCAGAGCACCTCCCCTC; *KDM4D (endogenous)* F-TCTGAGTCTGCCTTCTTCTG, R- GCCAGGGTTCACAAGTCCTGAG; *KDM4D (transgene)* F-TTGATGGACAAGCCTGTACC, R-TCATTTGCTGCCAGATCCTC. ; *APAK* F-TCCCTCGGAGAAATCAGGGA, R-TCCTTGTTCAGAGGGCAAGC; *BAX* F-TCT CCGGCGAATTGGAGATG, R-CCACGTCAGCAATCATCCTCT; Birc5 F-CCGATGACAACCCGATAGAGG, R-TGGCTCTCTGTCTGTCCAGT; *AKT1* F-CGCTTCTATGGTGCGGAGAT, R-GTTCTCCAGCTTCAGGTCCC; *BCL2* F-CGAGTGGGATGCTGGAGATG, R-GACGGTAGCGACGAGAGAAG

Histological studies and quantification CM dimensions and CM number in neonates. For histological analysis, hearts were fixed with 4% PFA. Paraffin sections were stained with H&E, Masson Trichrome, or immunostained using standard protocol with α-actinin (Sigma A7811), cardiac Troponin T (Thermo Scientific MS-295-P), BrdU (rat monoclonal; Abcam), cardiac troponin I (Abcam), and phospho-H3 (Abcam ab5176) antibodies, and Hoechst (Life Technologies H3570) to visualize nuclei. Images were acquired with wide field microscopy (Nikon A1R). To assess ACM transverse area, sections were stained with Wheat Germ Agglutinin (WGA, Life Technologies W6748), a marker for plasma membrane. Stitched-images of the whole left ventricle were acquired on a Nikon Ti-E scope. We chose several regions in each section at random, though we excluded large vessels, epicardium and endocardium, and

>1000 cells per animal were analyzed using Image J's "analyze particle" function (negative image of WGA stain), resulting in direct measurement of transverse area.

CM measurement method. Cardiomyocytes were isolated as described above. Cells were then fixed in 4% PFA for 15 min and imaged using a Zeiss Axiovert 200 microscope with Axiovision software. Intact cells from at least 8 images were then assessed using the measure function of ImageJ.

Myocardium and LV area quantification. Vibratome sections were cut from the mid-papillary muscle plane of hearts and imaged. Myocardium area and LV chamber area were manually traced in ImageJ and area was calculated using the "measure" tool.

Quantification of apoptosis. Apoptosis was visualized in vibratome sections by using a TUNEL staining kit (Life Technologies C10618) according to the manufacturer's guidelines. Following TUNEL labeling, we stained for WGA, Hoechst, and phalloidin, and imaged as described in the procedures for vibratome sections.

Immunohistochemistry and quantification in adult mice. For histological analysis, hearts were perfused and fixed with 4% PFA before paraffin embedding. 5 μm sections were deparaffinized and subjected to heat-mediated antigen retrieval by sodium citrate + 0.05% Tween-20, pH 6.0. Slides were then blocked with 2% normal donkey serum + 0.1% Triton X-100 before incubation with primary antibodies (phospho-H3 [Abcam, ab81299], Ki67 [Abcam, ab15580] and cardiac troponin T [Thermo Fisher, MS-295]) diluted in blocking buffer at 1:100 at 4°C overnight. Sections were then stained with the following secondary antibodies (Invitrogen) at 1:400 for 1h at room temperature: donkey anti-rabbit 488 (A32790), donkey anti-mouse 555 (A31570) and WGA 647 (W32466). Finally, sections were incubated with Hoescht (Thermo Fisher, H3570) at

1:2000 for 5 minutes before mounting with Mowiol. Images were acquired using a Leica Aperio Versa scanner. Quantification was performed using ImageJ. For baseline, an entire transverse section in the widest portion of the heart was quantified for each mouse. For injured hearts, 2 non-contiguous 1 mm^2 sections were counted and averaged in the infarct border and remote regions. Positive nuclei were distinguished by morphology and nearest co-stain (troponin T = cardiomyocyte, WGA = non-cardiomyocyte).

Statistics. All results are displayed as mean ± standard error of means. Graphpad Prism was used for one-way-ANOVAs and Tukey's post hoc tests performed on studies comparing more than two groups. Graphpad Prism was used for two-way-ANOVAs and Tukey's post hoc tests performed on studies with two independent variables. Microsoft Excel F-test and two-tailed T-test functions were used to analyze studies comparing two groups.

2.5 FIGURES

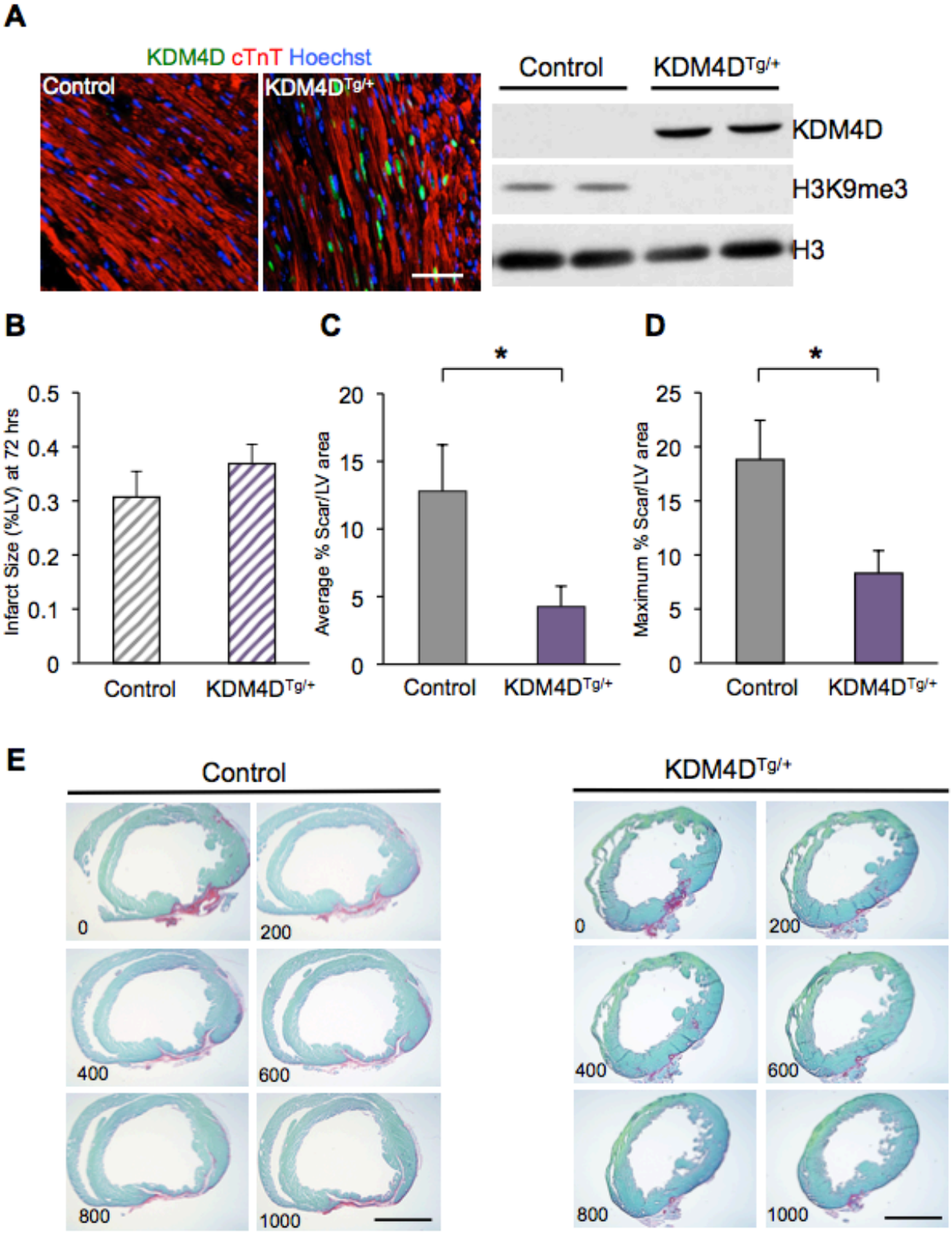
A
KDM4D cTnT Hoechst
Control
KDM4D^Tg/+
Control
KDM4D^Tg/+
KDM4D
H3K9me3
H3
B
Infarct Size (%LV) at 72 hrs
0.5
0.4
0.3
0.2
0.1
0
Control
KDM4D^Tg/+
C
*
Average % Scar/LV area
20
15
10
5
0
Control
KDM4D^Tg/+
D
*
Maximum % Scar/LV area
25
20
15
10
5
0
Control
KDM4D^Tg/+
E
Control
KDM4D^Tg/+
0
200
400
600
800
1000
0
200
400
600
800
1000

Figure 2.1: KDM4D extends the neonatal regenerative window. (A) Representative immunofluorescence image of cardiac sections (left) and immunoblotting of CM lysates (right) showing CM-specific exogenous KDM4D expression (anti-FLAG antibody to FLAG-tagged KDM4D) in KDM4D$^{Tg/+}$ hearts and depletion of H3K9me3. Green: KDM4D (FLAG-tag), red: cardiac troponin T (cTnT), blue: Hoechst. Scale bar: 50μm. (B) Quantification of TTC staining 3-days post-MI at P7 showing infarct size. (C-D) Quantification and (E) representative serial section images of hearts subjected to MI at P7 were analyzed by Sirius red/fast green staining of transverse sections 21 days after surgery (n=6), and KDM4D$^{Tg/+}$ (n=6) heart. Values are the mean ± SE. *P < 0.05. (E) Green area: myocardium, red area: scar tissue. Numbers in the bottom left corner of the serial sections indicate the distance in μm from the infarct site, with 0 being the site of the ligature placement. Scale bar: 2mm.

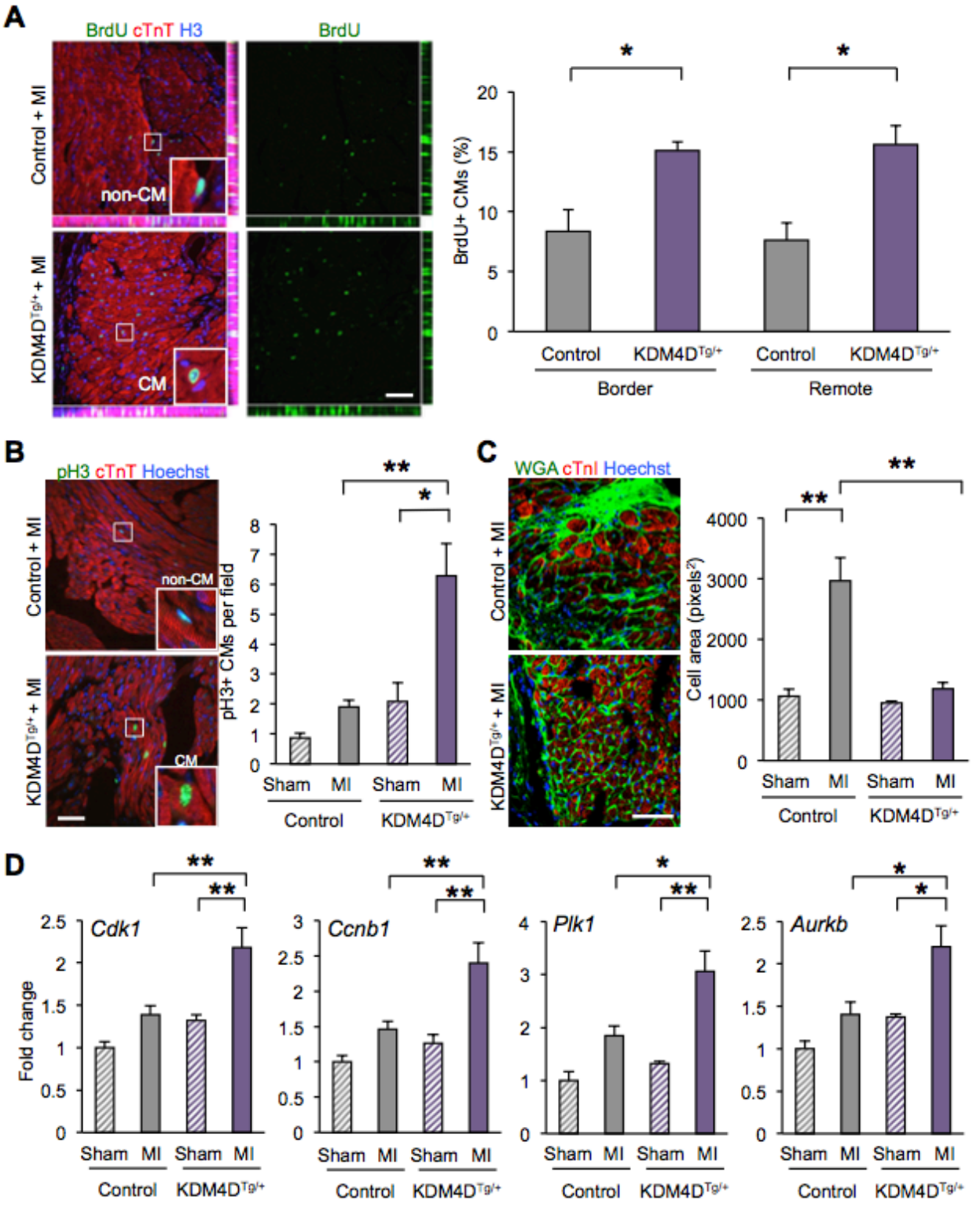
A
BrdU cTnT H3
BrdU
Control + MI
KDM4D^Tg/+ + MI
non-CM
CM
BrdU+ CMs (%)
Control
KDM4D^Tg/+
Border
Remote
B
pH3 cTnT Hoechst
pH3+ CMs per field
Sham
MI
C
WGA cTnI Hoechst
Cell area (pixels²)
D
Cdk1
Ccnb1
Plk1
Aurkb
Fold change

Figure 2.2: KDM4D potentiates CM proliferation in response to MI at P7. (A) High-resolution confocal microscopy images quantification demonstrating the effects of MI on BrdU staining at 21 days post-MI performed on P7 control and KDM4D$^{Tg/+}$ hearts. Green: BrdU, red: cTnT, blue: Histone H3. Inset: higher magnification image. The quantitative analysis represents the counting of multiple fields from control (n=4) and KDM4D$^{Tg/+}$ (n=3) hearts. Scale bar: 50μm. *P < 0.05. (B) High-resolution confocal microscopy images demonstrating the effects of MI on pH3 staining at seven days post-MI performed on P7 control (sham), control (MI), KDM4D$^{Tg/+}$ (sham), and KDM4D$^{Tg/+}$ (MI) hearts. Green: pH3, red: cTnT, blue: Hoechst. Inset: higher magnification image. Quantitative analysis represents counting of multiple fields from control (sham) (n=5), control (MI) (n=5), KDM4D$^{Tg/+}$ (sham) (n=5), and KDM4D$^{Tg/+}$ (MI) (n=6) hearts. Scale bar: 50μm. *P < 0.05, **P < 0.01. (C) Representative images and quantification of the effects of MI on cell size in control (sham) (n=5), control (MI) (n=6), KDM4D$^{Tg/+}$ (sham) (n=5) and KDM4D$^{Tg/+}$ (MI) (n=6) heart. Hearts were subjected to LAD ligation at seven days old and analyzed by Wheat germ agglutinin staining (WGA) staining of transverse sections 21 days after surgery. Green: WGA, red: cardiac troponin I, blue: Hoechst. Values are the mean ± SE. **P < 0.01. Scale bar: 50μm. (D) qRTPCR analysis of cell cycle gene RNA expression in CMs 7 days post-MI or sham operation performed in control and KDM4D$^{Tg/+}$ mice. All data were normalized to *Gapdh*. Control (sham): n=9, control (MI): n=8, KDM4D$^{Tg/+}$ (sham): n=6, KDM4D$^{Tg/+}$ (MI): n=10. Values are the mean ± SE. *P < 0.05, **P < 0.01.

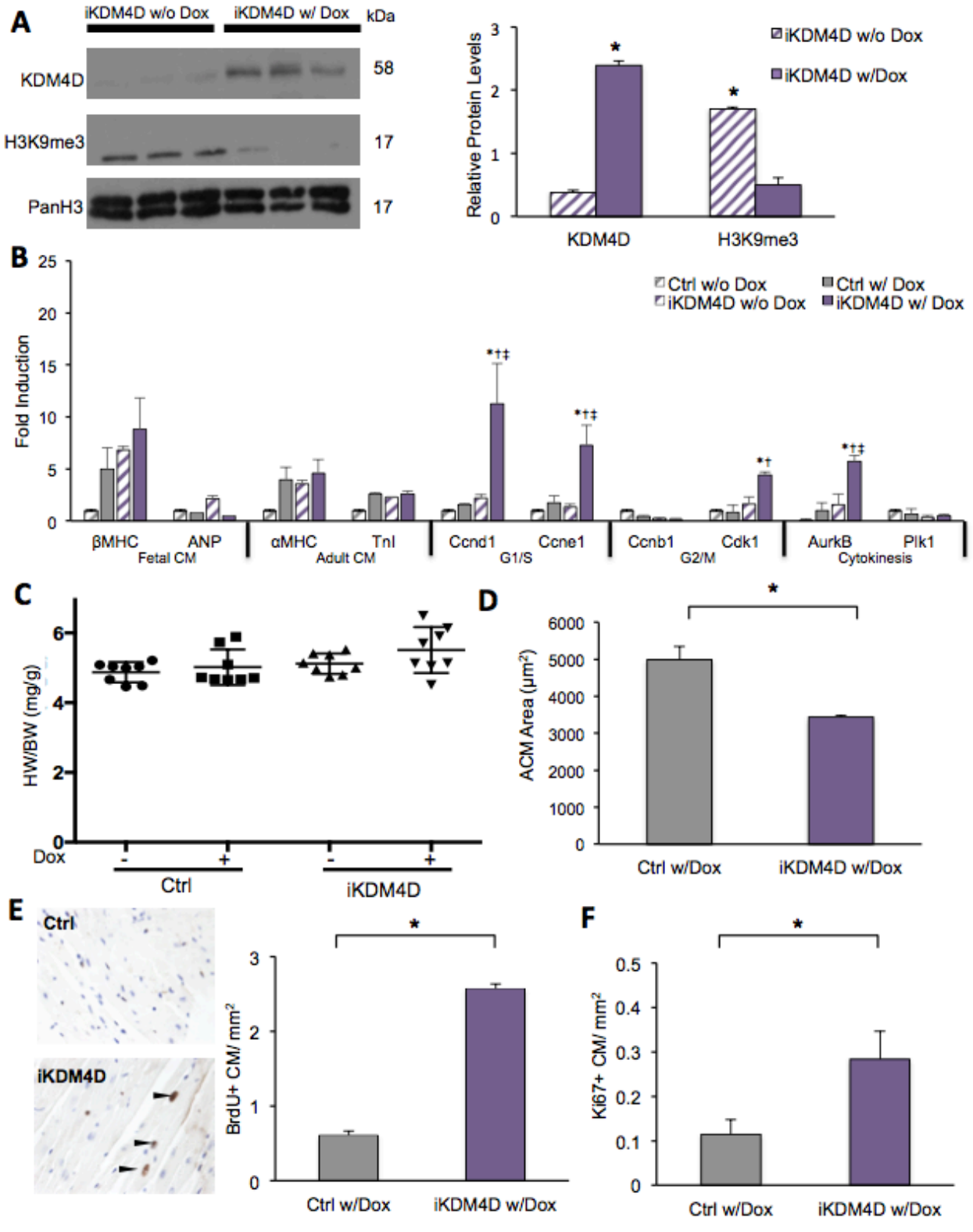
A
iKDM4D w/o Dox
iKDM4D w/ Dox
kDa
KDM4D
58
H3K9me3
17
PanH3
17
Relative Protein Levels
iKDM4D w/o Dox
iKDM4D w/Dox
KDM4D
H3K9me3
B
Fold Induction
Ctrl w/o Dox
Ctrl w/ Dox
iKDM4D w/o Dox
iKDM4D w/ Dox
βMHC
ANP
αMHC
TnI
Ccnd1
Ccne1
Ccnb1
Cdk1
AurkB
Plk1
Fetal CM
Adult CM
G1/S
G2/M
Cytokinesis
C
HW/BW (mg/g)
Dox
Ctrl
iKDM4D
D
ACM Area (μm²)
Ctrl w/Dox
iKDM4D w/Dox
E
Ctrl
iKDM4D
BrdU+ CM/ mm²
Ctrl w/Dox
iKDM4D w/Dox
F
Ki67+ CM/ mm²
Ctrl w/Dox
iKDM4D w/Dox

Figure 2.3: Characterization of KDM4D induction in ACMs. (A) Immunoblotting of ACM lysates (left) showing CM-specific KDM4D protein induction in iKDM4D hearts and depletion of H3K9me3 with two weeks of induction in ACMs. Densitometry analysis (right) shows KDM4D, and H3K9me3 levels relative to PanH3 control in iKDM4D CMs with (n=3) and iKDM4D CMs without (n=3) doxycycline induction. * P<0.05. (B) Expression of CM and cell cycle genes in isolated ACMs measured by qRT-PCR; fold induction vs. control (-Dox), expression normalized to *Gapdh*. (C) HW/BW quantification in uninduced control and iKDM4D mice (-Dox) and induced in control and iKDM4D (+Dox). (D) Quantification of ACM area (μm2), isolated 12-wk CMs control, and iKDM4D (+Dox). (E) BrdU staining (left), bar=100 μm; and quantification (right) in cardiac sections of control and iKDM4D (+Dox). Black arrowheads point to BrdU+ ACM nuclei. (F) Cell cycling marker Ki67 quantification in control and iKDM4D (+Dox) hearts. Sample Number: (A) iKDM4D (-Dox) = 3, iKDM4D (+Dox) = 3. (B) All groups = 8 (C) Control (+Dox) = 3, iKDM4D (+Dox) = 3 (D-F) ≥3 animals per group. Statistics: (A) Two-tailed t-test, iKDM4D (-Dox) vs. iKDM4D (+Dox), *P < 0.05. (B) Two-way ANOVA/Tukey's test, *P < 0.05 vs. ctrl (Dox), †P < 0.05 vs. iKDM4D (-Dox), ‡P < 0.05 vs. ctrl (+Dox). (C) Two-way ANOVA/Tukey's test, P > 0.05 vs. Control (-Dox). (D) Two-tailed t-test, control (+Dox) vs. iKDM4D (+Dox), *P < 0.05. (D) (E-F) Two-tailed t-test, ctrl (+Dox) vs. iKDM4D (+Dox), *P < 0.05.

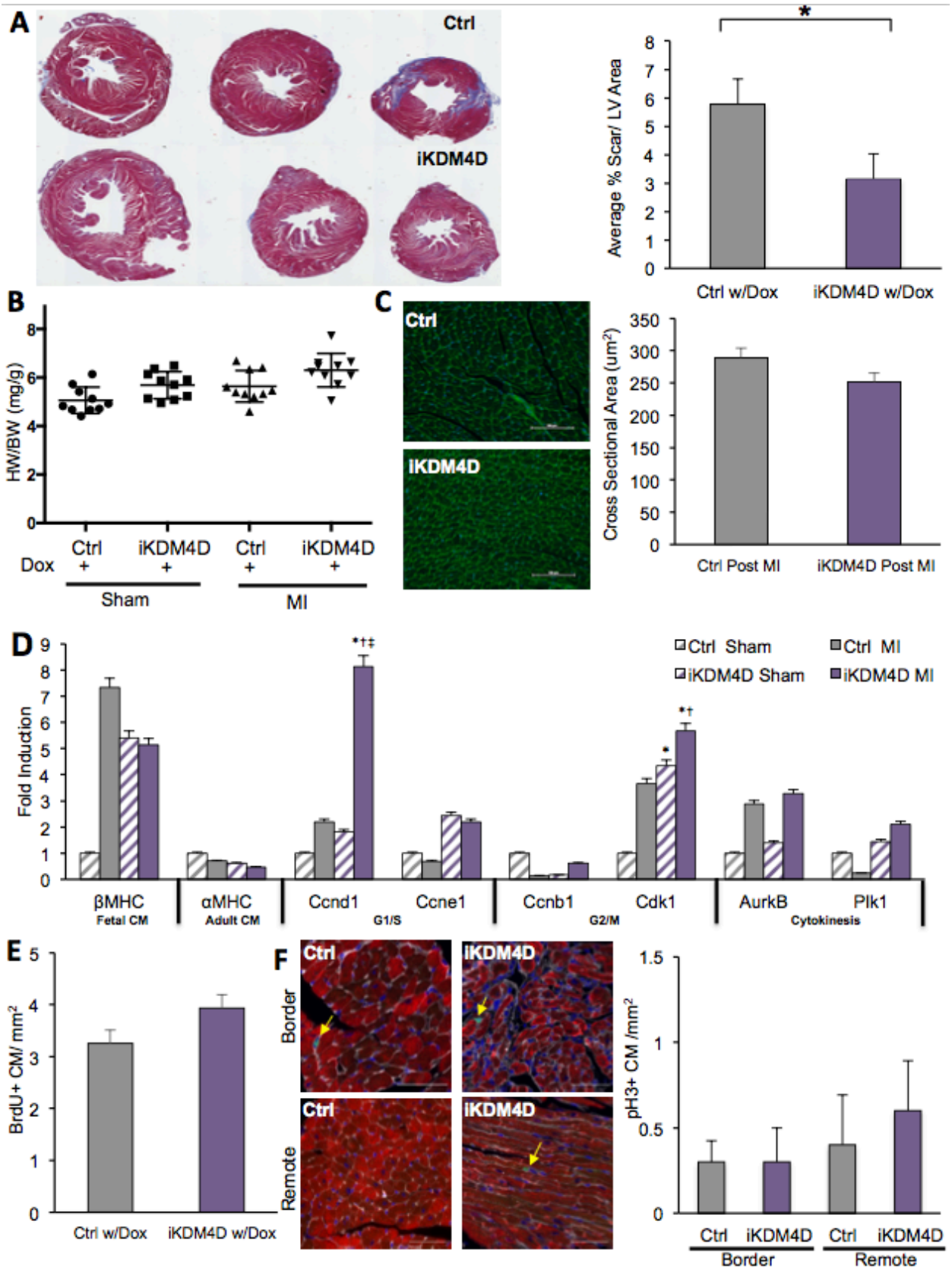
A
Ctrl
iKDM4D
Average % Scar/ LV Area
Ctrl w/Dox
iKDM4D w/Dox
B
HW/BW (mg/g)
Dox
Ctrl
iKDM4D
Ctrl
iKDM4D
Sham
MI
C
Ctrl
iKDM4D
Cross Sectional Area (um²)
Ctrl Post MI
iKDM4D Post MI
D
Fold Induction
Ctrl Sham
Ctrl MI
iKDM4D Sham
iKDM4D MI
βMHC
Fetal CM
αMHC
Adult CM
Ccnd1
Ccne1
G1/S
Ccnb1
Cdk1
G2/M
AurkB
Plk1
Cytokinesis
E
BrdU+ CM/ mm²
Ctrl w/Dox
iKDM4D w/Dox
F
Border
Remote
Ctrl
iKDM4D
pH3+ CM /mm²
Ctrl
iKDM4D
Ctrl
iKDM4D
Border
Remote

Figure 2.4: KDM4D induction reduces infarct scar size 14 days post-MI. (A) 4x magnification image of trichrome stained hearts (left) red: viable myocardium, blue: scar tissue. Quantification of infarct scar size (right) at two weeks post-MI in control vs. iKDM4D mice. (B) HW/BW quantification in induced control and iKDM4D (sham or MI) mice. (C) Left, WGA staining in post-MI induced control and iKDM4D PFA-fix hearts, bar = 100μm. Right, quantification of the ACM cross-sectional area. (D) Expression of CM and cell cycle genes in isolated ACMs measured by qRT-PCR, fold induction vs. control (sham), expression normalized to *Gapdh*. (E) BrdU staining quantification of cardiac sections of induced control and iKDM4D. (F) Cell cycling marker pH3 staining in control and iKDM4D (+Dox) post-MI hearts, border, and remote to infarct zone (left). Scale bar: 100 μm. Green: pH3, red: cTnT, blue: Hoechst. Quantitative analysis (right) of pH3 positive CMs per mm2. Sample Number: (A-F) ≥5 animals per group. Statistics: (A) Two-tailed t-test, ctrl (+Dox) vs. iKDM4D (+Dox), *$P < 0.05$. (B) Two-way ANOVA/Tukey's test, $P > 0.05$ vs. control (+Dox/sham) (C) Two-tailed t-test, control (post-MI) vs. iKDM4D (post-MI), $P > 0.05$. (D) Two-way ANOVA/Tukey's test, *$P < 0.05$ vs. ctrl (sham), †$P < 0.05$ vs. iKDM4D (sham), ‡$P < 0.05$ vs. ctrl (MI). (E) Two-tailed t-test, ctrl (+Dox) vs. iKDM4D (+Dox), $P > 0.05$. (F) Two-way ANOVA/Tukey's test, $P > 0.05$.

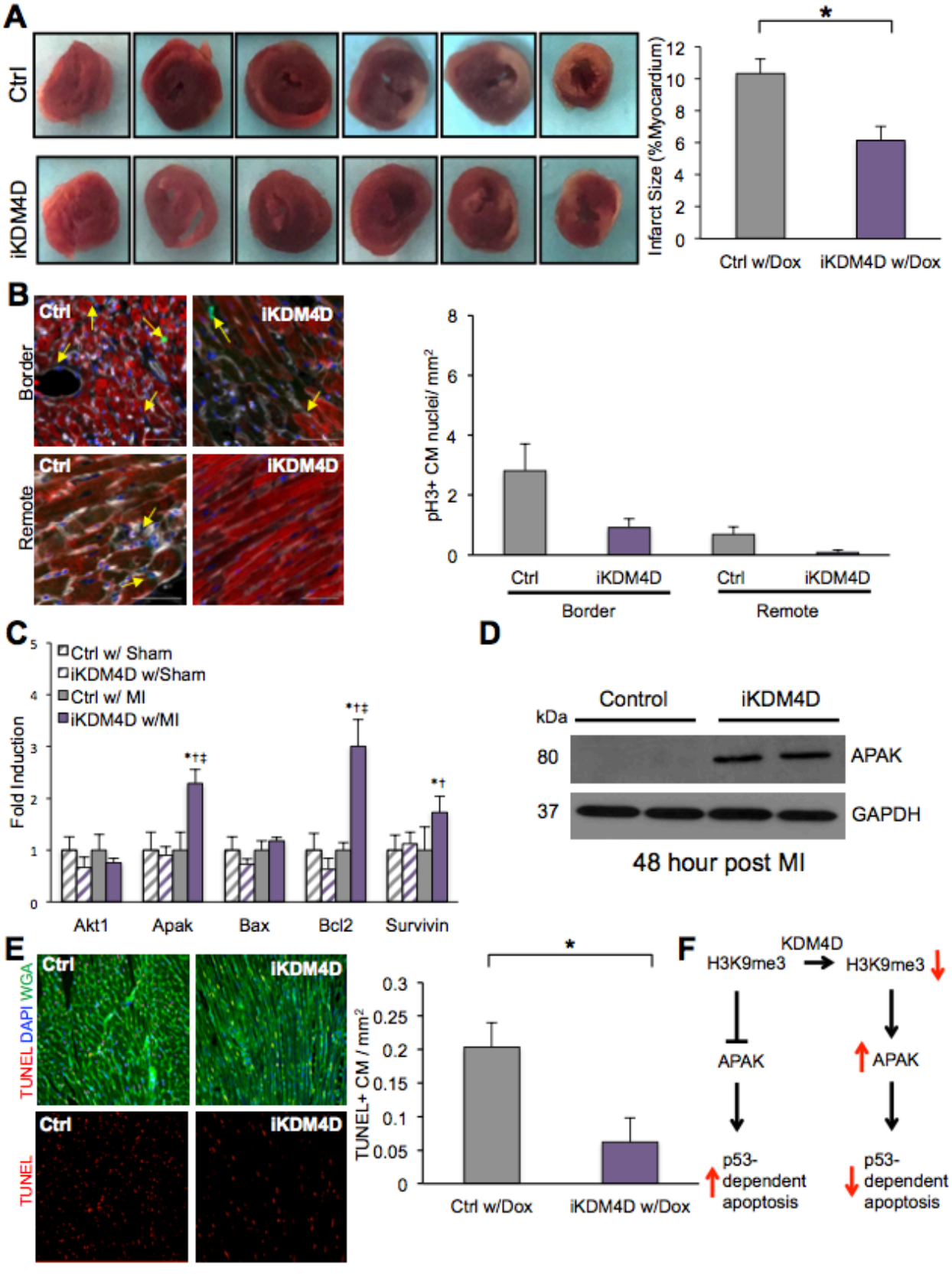
A
Ctrl
iKDM4D
Infarct Size (%Myocardium)
Ctrl w/Dox
iKDM4D w/Dox
B
Border
Remote
Ctrl
iKDM4D
pH3+ CM nuclei/ mm²
Border
Remote
C
Ctrl w/ Sham
iKDM4D w/Sham
Ctrl w/ MI
iKDM4D w/MI
Fold Induction
Akt1
Apak
Bax
Bcl2
Survivin
D
Control
iKDM4D
kDa
80
APAK
37
GAPDH
48 hour post MI
E
TUNEL DAPI WGA
TUNEL
TUNEL+ CM / mm²
Ctrl w/Dox
iKDM4D w/Dox
F
KDM4D
H3K9me3
H3K9me3
APAK
APAK
p53-dependent apoptosis
p53-dependent apoptosis

Figure 2.5: KDM4D induction mitigates acute myocardial injury 48hrs post-MI. (A) Representative images (left) of 2,3,5-triphenyl tetrazolium chloride (TTC) staining to visualize ischemic zone showed more significant areas of ischemic damage in induced control hearts than in induced iKDM4D hearts 48 hours after MI. Red: viable myocardium, Pale: hypoxic myocardium. Quantification (right) of infarct scar size (% myocardium) at 48hrs post-MI in control vs. iKDM4D animals. (B) Immunostaining and quantification of cell cycle marker pH3 48 hrs post-MI. (C) Expression of genes responsible for apoptosis and survival regulation in isolated ACMs measured by qRT-PCR, fold induction vs. control (sham), expression normalized to *Gapdh*. (D) Immunoblotting of ACM lysates showing an increase in anti-apoptotic APAK protein in iKDM4D hearts 48 hrs post-MI vs. controls. (E) Representative images of TUNEL staining in 48 hrs post-MI cardiac sections in control and iKDM4D animals (left). Quantification of TUNEL positive CMs per mm2. (F) Schematic representation of the proposed model. H3K9me3 represses cellular APAK levels, which in turn leads to increases in p53-dependent apoptosis. However, a decrease in H3K9me3 levels via KDM4D induction subsequently leads to increased APAK expression resulting in a reduction in p53-dependent apoptosis. Sample Number: (A) Ctrl (+Dox) = 3, iKDM4D (+Dox) = 3 (B) Border: Ctrl = 8, iKDM4D = 8; Remote: Ctrl =8, iKDM4D = 8 (C) Ctrl (sham) = 3, iKDM4D (sham) = 4, Ctrl (MI) = 4, iKDM4D (MI) = 5 (D) Ctrl= 3, iKDM4D= 3. Statistics: (A) Two-tailed t-test, ctrl (+Dox) vs. iKDM4D (+Dox), *P < 0.05. (B) Two-way ANOVA/Tukey's test, P > 0.05 vs. Control (border) (C) Two-way ANOVA/Tukey's test, *P < 0.05 vs. ctrl (sham), †P < 0.05 vs. iKDM4D (sham), ‡P < 0.05 vs. ctrl (MI). (E) Two-tailed t-test, ctrl (+Dox) vs. iKDM4D (+Dox), *P < 0.05.

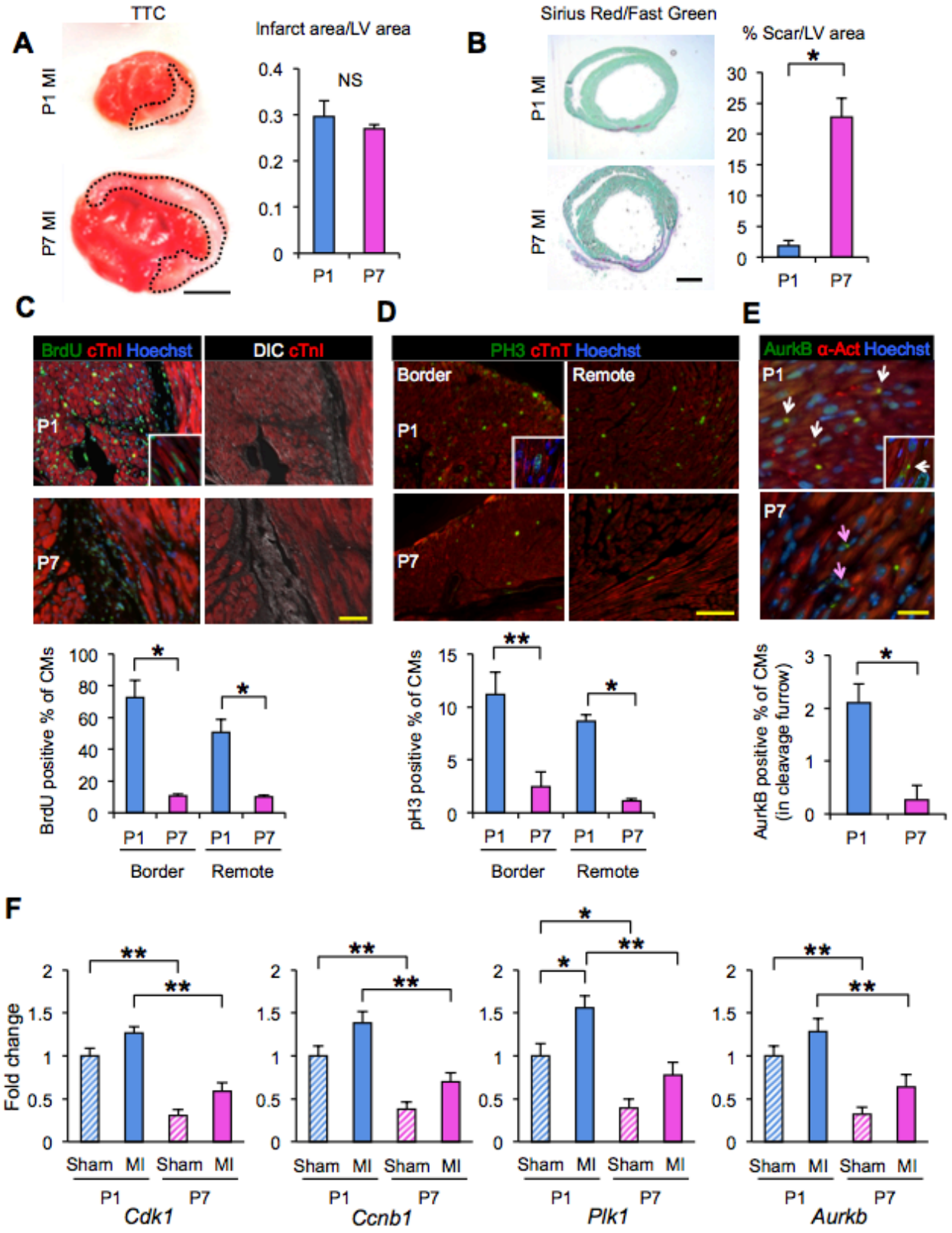
A
TTC
P1 MI
P7 MI
Infarct area/LV area
NS
0.4
0.3
0.2
0.1
0
P1
P7
B
Sirius Red/Fast Green
P1 MI
P7 MI
% Scar/LV area
*
30
25
20
15
10
5
0
P1
P7
C
BrdU cTnI Hoechst
DIC cTnI
P1
P7
D
PH3 cTnT Hoechst
Border
Remote
P1
P7
E
AurkB α-Act Hoechst
P1
P7
BrdU positive % of CMs
100
80
60
40
20
0
*
*
P1
P7
P1
P7
Border
Remote
pH3 positive % of CMs
15
10
5
0
**
*
P1
P7
P1
P7
Border
Remote
AurkB positive % of CMs (in cleavage furrow)
3
2
1
0
*
P1
P7
F
Fold change
2
1.5
1
0.5
0
**
**
Sham
MI
Sham
MI
P1
P7
Cdk1
Ccnb1
Plk1
Aurkb

Figure S2.1: P1 mice display reduced scar and increased CM cell cycling 21 days after MI. (A) Staining of hearts with 2,3,5-triphenyl tetrazolium chloride (TTC) to visualize ischemic zone showed equivalent areas of ischemic damage in P1 (n=5) and P7 (n=4) hearts 72 hrs after MI. Red area: viable myocardium, white area: dead. Values are the mean ± SE. NS (not significant). Scale bar: 1mm. The dashed area shows the infarct zone. (B) Sirius Red/Fast Green staining and quantification of infarct size at P21 (n=3 per group). Scale bar: 1mm. Values are the mean ± SE. $*P < 0.05$. (C-E) Immunostaining (above) and quantification (below) of cell cycle markers (C) BrdU at P21, (D) pH3 7-days after MI, and (E) Aurora Kinase B (AurkB) 7-days after MI. Insets show cycling CMs double positive for CM and cell cycle markers. White arrows point to CMs; pink arrows point to non-CMs. Quantitative analysis of cell cycle markers represents the counting of multiple fields from three independent samples per group. Values are the mean ± SE. $*P < 0.05$, $**P < 0.01$. Scale bars: (C and E) 50μm, (D) 100μm. (F) CM RNA expression analysis demonstrating the effects of surgery on cell cycle genes 7 days post-MI or sham operation performed on P1 and P7 hearts. All data normalized by *Gapdh*. P1 (sham): n=6, P1 (MI): n=7, P7 (sham): n=7, P7 (MI): n=6. Values are the mean ± SE. $*P < 0.05$, $**P < 0.01$.

A

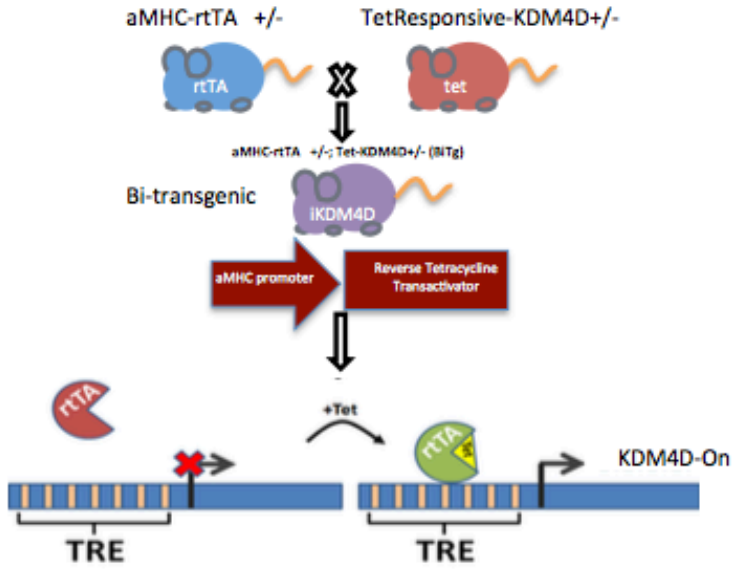

B

Control groups:

- Non-BiTg mice (WT and Single Tg's)

Experimental Group:

- BiTg mice, KDM4D induction via doxycycline treatment

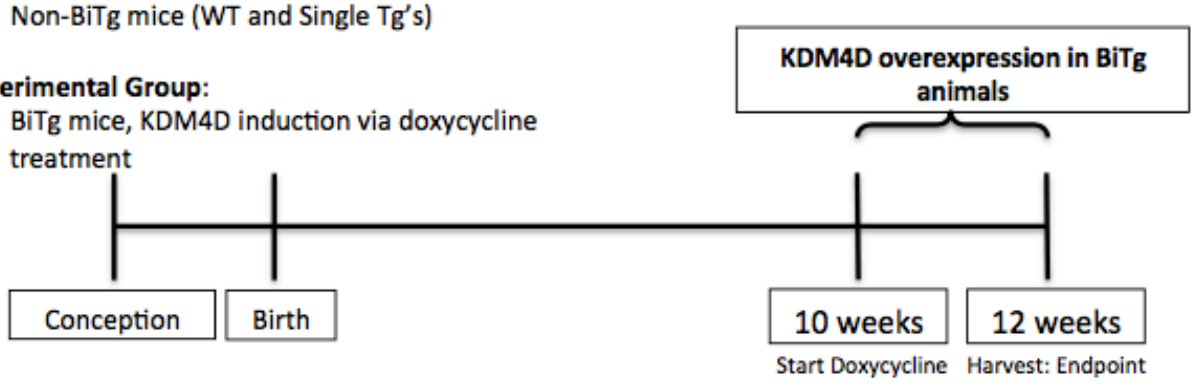

C

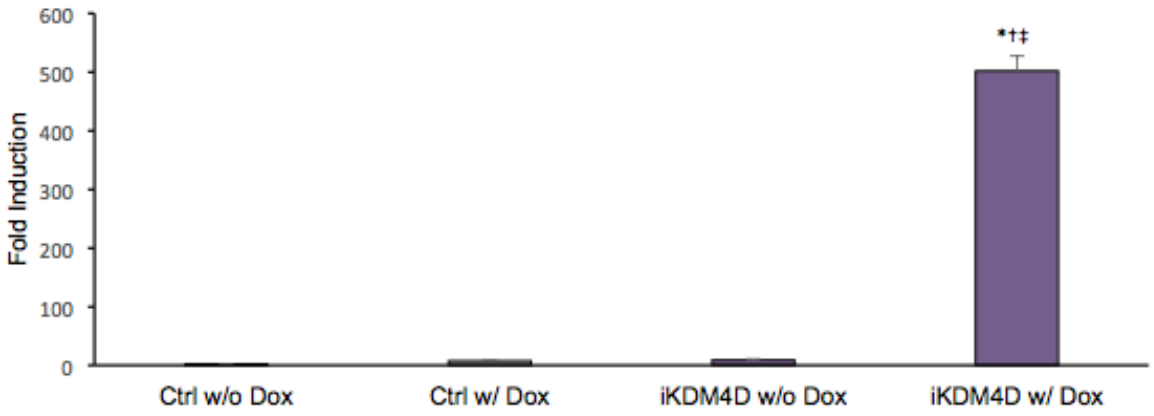

Figure S2.2: Inducible KDM4D mouse model construction, induction protocol, and KDM4D gene expression levels relative to GAPDH. (A) Schematic showing breeding strategy resulting in iKDM4D mice, and KDM4D induction in ACMs. (B) Timeline showing protocol for ACM-specific KDM4D expression and endpoints. (C) KDM4D transgene expression is robustly induced in iKDM4D ACMs fold induction vs. control (-Dox), expression normalized to *Gapdh. Sample Number: (*C) ≥ 5 animals per group. *Statistics:* Two-way ANOVA/Tukey's test, * $P<0.05$ vs. ctrl (-Dox), † $P<0.05$ vs. ctrl (+Dox), ‡ $P<0.05$ vs. iKDM4D (-Dox).

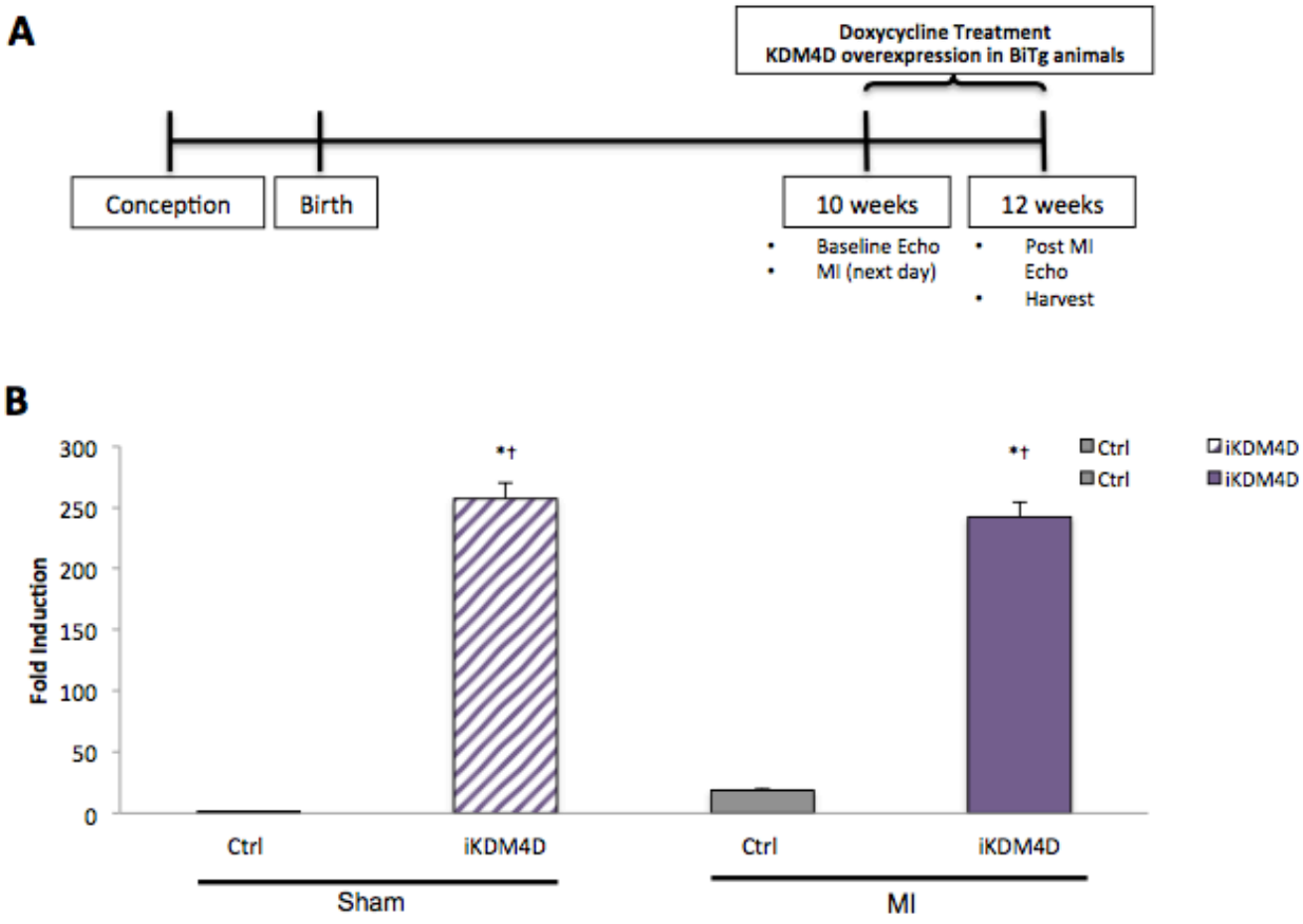
A
Doxycycline Treatment
KDM4D overexpression in BiTg animals
Conception
Birth
10 weeks
12 weeks
Baseline Echo
MI (next day)
Post MI Echo
Harvest
B
Fold Induction
300
250
200
150
100
50
0
*†
*†
Ctrl
iKDM4D
Ctrl
iKDM4D
Sham
MI
Ctrl
Ctrl
iKDM4D
iKDM4D

Figure S2.3: Inducible KDM4D mouse MI protocol, and KDM4D gene expression levels relative to GAPDH. (A) Timeline showing protocol for development-restricted KDM4D expression in ACMs. (B) KDM4D transgene expression is induced in iKDM4D ACMs fold induction vs. control (sham), expression normalized to *Gapdh*. *Sample Number:* (C) ≥ 5 animals per group. *Statistics:* Two-way ANOVA/Tukey's test, * $P<0.05$ vs. ctrl (sham), † $P<0.05$ vs. ctrl (MI).

2.6 TABLE

Table 2.1: Cardiac function and morphology in KDM4D MI-operated mice. Echocardiography results in 12-week old mice, 14 days post-operation. HR: Heart Rate, EF: Ejection Fraction, FS: Fractional Shorting, LVESV: Left Ventricular End-Systolic Volume, LVEDD: Left Ventricular End-Diastolic Dimension, LVPW: Left Ventricular Posterior Wall Thickness. Mean, and SEM values are shown. Sample Number: Sham, Control=4, iKDM4D=4; MI, Control=8, iKDM4D=9. Statistics: Two-way ANOVA/Tukey's test, control (MI) vs. iKDM4D (MI), * P<0.05.

	Control		iKDM4D	
	Sham	**MI**	**Sham**	**MI**
HR (BPM)	572.42 ± 22.41	584.74 ± 12.89	540.69 ± 39.95	451.29 ± 32.34*
EF (%)	88.91 ± 2.06	30.25 ± 1.69	86.86 ± 2.39	50.80 ± 6.02*
FS (%)	58.58 ± 3.76	13.90 ± 0.81	57.00 ± 4.03	26.78 ± 4.33*
LVESV (uL)	4.07 ± 0.87	45.77 ± 9.51	5.79 ± 1.16	30.89 ± 7.56
LVEDD (mm)	3.02 ± 0.06	3.75 ± 0.28	3.30 ± 0.16	3.57 ± 0.29
LVPW;d (mm)	0.77 ± 0.07	0.57 ± 0.09	0.71 ± 0.02	0.67 ± 0.08

2.7 BIBLIOGRAPHY - CHAPTER 2

1. Laflamme, M. A. & Murry, C. E. Heart regeneration. *Nature* **473,** 326–335 (2011).

2. Bergmann, O. *et al.* Evidence for cardiomyocyte renewal in humans. *Science* **324,** 98 (2009).

3. Bergmann, O. *et al.* Dynamics of Cell Generation and Turnover in the Human Heart. *Cell* **161,** 1566–1575 (2015).

4. Senyo, S. E. *et al.* Mammalian heart renewal by pre-existing cardiomyocytes. *Nature* **493,** 433–6 (2013).

5. Sereti, K.-I. *et al.* Analysis of cardiomyocyte clonal expansion during mouse heart development and injury. *Nat. Commun.* **9,** 754 (2018).

6. Porrello, E. R. *et al.* Transient regenerative potential of the neonatal mouse heart. *Science* **331,** 1078–80 (2011).

7. Porrello, E. R. *et al.* Regulation of neonatal and adult mammalian heart regeneration by the miR-15 family. *Proc. Natl. Acad. Sci. U. S. A.* **110,** 187–92 (2013).

8. Oyama, K., El-Nachef, D. & Maclellan, W. R. Regeneration potential of adult cardiac myocytes. *Cell Res.* **23,** (2013).

9. Mahmoud, A. I. *et al.* Meis1 regulates postnatal cardiomyocyte cell cycle arrest. *Nature* **497,** 249–253 (2013).

10. Xin, M. *et al.* Hippo pathway effector Yap promotes cardiac regeneration. *Proc. Natl. Acad. Sci.* **110,** 13839–13844 (2013).

11. Ahuja, P., Sdek, P. & MacLellan, W. R. Cardiac myocyte cell cycle control in development, disease, and regeneration. *Physiol. Rev.* **87,** 521–44 (2007).

12. Zhong, W. *et al.* Hypertrophic growth in cardiac myocytes is mediated by Myc through a Cyclin D2-dependent pathway. *EMBO J.* **25,** 3869–3879 (2006).

13. Xiao, G. *et al.* Inducible activation of c-Myc in adult myocardium in vivo provokes cardiac myocyte hypertrophy and reactivation of DNA synthesis. *Circ. Res.* **89,** 1122–9 (2001).

14. Sdek, P. *et al.* Rb and p130 control cell cycle gene silencing to maintain the postmitotic phenotype in cardiac myocytes. *J. Cell Biol.* **194,** 407–23 (2011).

15. Soonpaa, M. H. *et al.* Cyclin D1 overexpression promotes cardiomyocyte DNA synthesis and multinucleation in transgenic mice. Cyclin D1 Overexpression Promotes Cardiomyocyte DNA Synthesis and Multinucleation in Transgenic Mice. *J. Clin. Invest* **99,** 2644–2654 (1997).

16. Freeman, Miles D et al. “Inactivation of chromatin remodeling factors sensitizes cells to selective cytotoxic stress.” *Biologics: targets & therapy* vol. **8** 269-80. 14 Nov. (2014).

17. Chen T, Dent SY. Chromatin modifiers and remodellers: regulators of cellular differentiation. Nat Rev Genet. 2014;15 (2):93–106.

18. Kooistra, S., Helin, K. Molecular mechanisms and potential functions of histone demethylases. Nat Rev Mol Cell Biol 13, 297–311 (2012).

19. El-Nachef, D. *et al.* Repressive histone methylation regulates cardiac myocyte cell cycle exit. *J. Mol. Cell. Cardiol.* **121,** 1–12 (2018).

20. Olcina, M., Leszczynska, K., Senra, J. et al. H3K9me3 facilitates hypoxia-induced p53-dependent apoptosis through repression of APAK. Oncogene 35, 793–799 (2016).

21. Kim, Tae-Dong et al. “Regulation of tumor suppressor p53 and HCT116 cell physiology by histone demethylase JMJD2D/KDM4D.” PloS one vol. **7**,4 (2012)

22. Khoury-Haddad, Hanan et al. “PARP1-dependent recruitment of KDM4D histone demethylase to DNA damage sites promotes double-strand break repair.” Proceedings of the National Academy of Sciences of the United States of America vol. **111**,7 (2014)

23. Ayrapetov, Marina K et al. “DNA double-strand breaks promote methylation of histone H3 on lysine 9 and transient formation of repressive chromatin.” Proceedings of the National Academy of Sciences of the United States of America vol. **111**,25 (2014)

24. Khoury-Haddad, Hanan et al. “The emerging role of lysine demethylases in DNA damage response: dissecting the recruitment mode of KDM4D/JMJD2D to DNA damage sites.” Cell cycle (Georgetown, Tex.) vol. **14**,7 (2015): 950-8.

25. Valencik ML, McDonald JA. Codon optimization markedly improves doxycycline regulated gene expression in the mouse heart. Transgenic Res. 2001 Jun; 10(3): 269-75.

26. Heallen, T. R., Kadow, Z. A., Kim, J. H., Wang, J. & Martin, J. F. Stimulating Cardiogenesis as a Treatment for Heart Failure. *Circ. Res.* **124,** 1647–1657 (2019).

27. Quaife-Ryan, Gregory A et al. “Multicellular Transcriptional Analysis of Mammalian Heart Regeneration.” Circulation vol. **136**,12 (2017): 1123-1139.

28. Lu, Chunwan et al. “Contrasting roles of H3K4me3 and H3K9me3 in regulation of apoptosis and gemcitabine resistance in human pancreatic cancer cells.” BMC cancer vol.

18,1 149. 6 Feb. (2018)

29. Biga, Peggy R et al. “Distribution of H3K27me3, H3K9me3, and H3K4me3 along autophagy-related genes highly expressed in starved zebrafish myotubes.” Biology open vol. **6**,11 1720-1725. 15 Nov. (2017)

30. Magaraki, Aristea et al. “Silencing markers are retained on pericentric heterochromatin during murine primordial germ cell development.” Epigenetics & chromatin vol. **10** 11. 11 Mar. (2017)

31. Pedersen, Marianne Terndrup et al. “Continual removal of H3K9 promoter methylation by Jmjd2 demethylases is vital for ESC self-renewal and early development.” The EMBO journal vol. **35**,14 (2016): 1550-64.

32. Mendelsohn AR, Larrick JW. Stem cell depletion by global disorganization of the H3K9me3 epigenetic marker in aging. Rejuvenation Res. (2015) **18**:371–5.

33. Lachner M, O'Carroll D, Rea S, Mechtler K, Jenuwein T. Methylation of histone H3 lysine 9 creates a binding site for HP1 proteins. Nature. (2001) **410**:116–20.

34. Nakayama J, Rice JC, Strahl BD, Allis CD, Grewal SI. Role of histone H3 lysine 9 methylation in epigenetic control of heterochromatin assembly. Science. (2001) **292**:110–3.

35. Becker, Justin S et al. “H3K9me3-Dependent Heterochromatin: Barrier to Cell Fate Changes.” Trends in genetics : TIG vol. **32**,1 (2016): 29-41.

36. Narita M, Nunez S, Heard E, Narita M, Lin AW, Hearn SA et al. Rb-mediated heterochromatin formation and silencing of E2F target genes during cellular senescence.

Cell 2003; **113**:703- 16.

37. Nielsen SJ, Schneider R, Bauer UM, Bannister AJ, Morrison A, O'Carroll D et al. Rb targets histone H3 methylation and HP1 to promoters. Nature 2001; **412**:561-5.

38. Olivetti G, Quaini F, Sala R, et al. Acute myocardial infarction in humans is associated with activation of programmed myocyte cell death in the surviving portion of the heart. J Mol Cell Cardiol. 1996;28:2005–16.

39. Abbate A, Biondi-Zoccai GG, Baldi A, et al. Increased myocardial apoptosis in patients with unfavorable left ventricular remodeling and early symptomatic post-infarction heart failure. *J Am Coll Cardiol*. 2003;41(5):753–60.

40. Baldi A, Abbate A, Di Sciascio G, et al. Apoptosis and post-infarction left ventricular remodeling. *J Mol Cell Cardiol*. 2002;34(2):165–74.

41. Chatterjee S, Stewart AS, Bish LT, Jayasankar V, Kim EM, Pirolli T, Burdick J, Woo YJ, Gardner TJ, Sweeney HL. Viral gene transfer of the antiapoptotic factor Bcl-2 protects against chronic postischemic heart failure. Circulation. 2002; 106: I212–I217.

42. Hochhauser E, Kivity S, Offen D, Maulik N, Otani H, Barhum Y, Pannet H, Shneyvays V, Shainberg A, Goldshtaub V, Tobar A, Vidne BA. Bax ablation protects against myocardial ischemia-reperfusion injury in transgenic mice. Am J Physiol Heart Circ Physiol. 2003; 284: H2351–H2359.

43. Imahashi K, Schneider MD, Steenbergen C, Murphy E. Transgenic expression of Bcl-2 modulates energy metabolism, prevents cytosolic acidification during ischemia, and reduces ischemia/reperfusion injury. Circ Res. 2004; 95: 734–741.

44. Hochhauser E, Cheporko Y, Yasovich N, Pinchas L, Offen D, Barhum Y, Pannet H, Tobar A, Vidne BA, Birk E. Bax deficiency reduces infarct size and improves long-term function after myocardial infarction. Cell Biochem Biophys. 2007; 47: 11–20.

45. Dohi T, Beltrami E, Wall NR, Plescia J, Altieri DC. Mitochondrial survivin inhibits apoptosis and promotes tumorigenesis. J Clin Invest. 2004; 114:1117-27

46. Altieri DC. Targeted therapy by disabling crossroad signaling networks: The survivin paradigm. Mol Cancer Ther. 2006 ;5:478-82

47. Tsang TJ, Hsueh YC, Wei EI, Lundy DJ, Cheng B, Chen YT, Wang SS, Hsieh PCH. Subcellular Localization of Survivin Determines Its Function in Cardiomyocytes. Theranostics 2017; 7(18):4577-4590.

48. Li F, Ambrosini G, Chu EY, Plescia J, Tognin S, Marchisio PC. et al. Control of apoptosis and mitotic spindle checkpoint by survivin. Nature. 1998;396:580-4

49. Yamagishi Y, Honda T, Tanno Y, Watanabe Y. Two histone marks establish the inner centromere and chromosome bi-orientation. Science. 2010;330:239-43

50. Kelly AE, Ghenoiu C, Xue JZ, Zierhut C, Kimura H, Funabiki H. Survivin reads phosphorylated histone h3 threonine 3 to activate the mitotic kinase aurora b. Science. 2010;330:235-9

51. Wang F, Dai J, Daum JR, Niedzialkowska E, Banerjee B, Stukenberg PT. et al. Histone h3 thr-3 phosphorylation by haspin positions aurora b at centromeres in mitosis. Science. 2010;330:231-5

52. Long, X et al. "p53 and the hypoxia-induced apoptosis of cultured neonatal rat cardiac

myocytes." The Journal of clinical investigation vol. 99,11 (1997): 2635-43. doi:10.1172/JCI119452

53. Matsusaka H et al. "Targeted deletion of p53 prevents cardiac rupture after myocardial infarction in mice." Cardiovascular Research, Volume 70, Issue 3, June 2006, Pages 457–465

54. Naito AT, et al. Promotion of CHIP-mediated p53 degradation protects the heart from ischemic injury. Circ. Res. 2010;106:1692–1702. doi: 10.1161/CIRCRESAHA.109.214346.

55. Levine A. p53, the cellular gatekeeper for growth and division. Cell. 1997; 88:323–331.

56. Agarwal ML, Taylor WR, Chernov MV, Chernova OB, Stark GR. The p53 network. J Biol Chem. 1998;273:1–4.

57. Innocente SA, Abrahamson JLA, Cogswell JP, Lee JM. p53 regulates a G2 checkpoint through cyclin B1. Proc Natl Acad Sci USA. 1999;96:2147–2152.

58. Haupt Y, Rowan S, Shaulian E, Vousden KH, Oren M. Induction of apoptosis in HeLa cells by transactivation-deficient p53. Genes Dev. 1995;9:2170–2183.

59. Miyashita T, Harigai M, Hanada M, Reed JC. Identification of a p53-dependent negative response element in the bcl-2 gene. Cancer Res. 1994;54:3131–3135.

60. Sano M, Minamino T, Toko H, Miyauchi H, Orimo M, Qin Y, Akazawa H, Tateno K, Kayama Y, Harada M, Shimizu I, Asahara T, Hamada H, Tomita S, Molkentin JD, Zou Y, Komuro I. p53-induced inhibition of Hif-1 causes cardiac dysfunction during pressure overload. Nature. 2007; **446**: 444–448.

61. Chunyan, Tian & Xing, Guichun & Xie, Ping & Lu, Kefeng & Nie, Jing & Wang, Jian & Li, Li & Gao, Mei & Zhang, Lingqiang & He, Fuchu. (2009). KRAB-type zinc-finger protein Apak specifically regulates p53-dependent apoptosis. Nature cell biology. 11. 580-91. 10.1038/ncb1864.

62. Tian C, Xing G, Xie P, et al. KRAB-type zinc-finger protein Apak specifically regulates p53-dependent apoptosis. Nature Cell Biology. 2009 May;11(5):580-591. DOI: 10.1038/ncb1864.

63. Zhang, Haoyue et al. ""Loss of H3K9me3 Correlates with ATM Activation and Histone H2AX Phosphorylation Deficiencies in Hutchinson-Gilford Progeria Syndrome."" PloS one vol. 11,12 e0167454. 1 Dec. 2016, doi:10.1371/journal.pone.0167454

64. Sun Y, Jiang X, Xu Y, et al. Histone H3 methylation links DNA damage detection to activation of the tumour suppressor Tip60. Nat Cell Biol. 2009;11(11):1376–1382. doi:10.1038/ncb1982

65. Sanbe, A. *et al.* Reengineering Inducible Cardiac-Specific Transgenesis With an Attenuated Myosin Heavy Chain Promoter. *Circ. Res.* **92,** 609–616 (2003).

66. Mahmoud, A. I., Porrello, E. R., Kimura, W., Olson, E. N. & Sadek, H. A. Surgical models for cardiac regeneration in neonatal mice. *Nat. Protoc.* **9,** 305–311 (2014).

Chapter 3. CARDIOMYOCYTE DEDIFFERTIATION AND PROLIFERATION VIA PARTIAL REPROGRAMMING

ABSTRACT

In mammals, fetal cardiac myocytes proliferate robustly, contributing to the growth of the heart in utero. However, only seven days after birth, cardiac myocytes become terminally differentiated, losing the ability to enter the cell cycle. After an injury such as myocardial infarction, the limited capacity of adult cardiac myocytes to proliferate and repopulate the damaged heart leads to progressive dysfunction and development of heart failure. Myocardial regeneration to restore cardiac muscle after an injury has been proposed as a means to prevent the development of heart failure. Therefore, developing strategies that promote the proliferation of endogenous cardiac myocytes after injury holds excellent promise as a therapeutic strategy. In this study, we aim to enhance the proliferative capacity of adult cardiac myocytes by dedifferentiating them in vivo. Reprogramming somatic cells to pluripotent stem cells is well established, but several reports suggest "partial" reprogramming is also possible. Utilizing the Yamanaka factors Oct4, Sox2, Klf4, and c-Myc (4F), we will attempt to reprogram adult cardiac myocytes, restoring their endogenous proliferative capacity. Thus, this study will utilize novel *in vivo* adult cardiac myocyte specific reprogramming models to address our knowledge gaps and potentially identify proliferative pathways amenable to directed therapies.

3.1 INTRODUCTION

More than 90 million American adults are living with some form of cardiovascular disease, while direct and indirect costs of cardiovascular diseases have soared to an estimated total of more than $329 billion annually[1]. The major component of this burden is heart failure (HF). The development of HF is due in part to the inability of adult cardiomyocytes (ACMs) to proliferate and repair the damaged heart. Current approaches to regenerate the myocardium have focused on using stem cells to repair damaged tissue. However, our group has proposed an alternative strategy. Instead of exogenous stem cells, we aim to manipulate endogenous ACMs to proliferate. Understanding the molecular blockades to ACM division or how to reinitiate CM proliferation is limited[2]. Still, our lab has focused on elucidating the mechanisms and identifying the barriers to CM proliferation. Our hypothesis of epigenetic mechanisms silencing cell cycle genes of ACMs represents a new paradigm in the field.

In 2006 the Yamanaka's lab described four transcription factors cable of reprogramming fully differentiated cells into inducible pluripotent stem cells[3] (iPSC). iPSCs are a type of pluripotent stem cell that can be generated directly from a somatic cell. Pluripotent stem cells hold great promise in the field of regenerative medicine because they can propagate indefinitely, as well as give rise to every other cell type in the body, including CMs.

Cellular reprogramming can be achieved by forced expression of Yamanaka factors *Oct4*, *Sox2*, *Klf4*, and *c-Myc* (4F) through the global induction of shifts in the epigenetic landscape of cells[3]. *Oct4*, *Sox2*, and *KLF4* function together to activate target genes and establish a pluripotent transcription factor network and epigenome. c-Myc works to enhance the accessibility of target genes by stimulating DNA replication (**Figure 3.1**). Many of the epigenetic marks that are remodeled during cellular reprogramming (e.g. DNA methylation and post-translational

modification of histones) are present in ACMs. In fact, stable epigenetic silencing of cell cycle genes in ACMs has emerged as a hallmark of the terminal differentiation process in CMs.

In 2010, a paper was published challenging the idea that cardiomyocytes are permanently terminally differentiated[4]. They found that postnatal mammalian cardiomyocytes are instead potentially cable of plasticity in culture. Dedifferentiation of myocytes was proven to facilitate proliferation, conferring a degree of stemness, including the expression of stem cell antigen c-kit. Another study further characterized the cellular process of dedifferentiation, proliferation, and redifferentiation of adult mammalian cardiomyocytes in *vitro*[5](**Figure 3.2)**. They determined that ACMs following an injury undergo a dedifferentiation process expressing the stemness markers *Runx1* and *Dab2* peaking in expression about three days post-injury. Dedifferentiation is then followed by ACM expression of proliferation markers ki67 and pH3 by the 5th-day post-injury. Finally, with redifferentiation markers peaking by day 7. These studies have highlighted the potential of dedifferentiating CMs to proliferate them *in vitro*.

In 2016 the Belmonte group published a study suggesting that the global induction of 4F *in vivo* is cable of inducing an expansion of muscle stem cells in aged mice, improving muscle regeneration after injury[6]. This same study also showed that the induction of 4F in a premature aging mouse model, partially rescued the degeneration of vascular smooth muscle cells and normalizing EKG analysis compared to control mice.

Groups have reported that partial reprogramming *in vitro* by transient expression of 4F can induce a dedifferentiated progenitor-like state in non-CMs. However, we believe that the complexities of the cardiomyocyte cell cycle demand an *in vivo* approach to understanding better how reprogramming may affect differentiation and proliferation of ACMs.

3.2 RESULTS

3.2.1 *ACM-specific 4F reprogramming factor induction mouse model.*

This study aimed to determine if overexpressing 4F in ACMs could drive proliferative potential after injury. We tested this hypothesis by subjecting adult inducible 4F expressing hearts to ischemic injury via myocardial infarction (MI). To generate a CM-specific mouse model, we crossbreed a rtTA line[7], driven by an alpha myosin heavy chain promoter with a 4F tet line[8]. This breeding produced inducible 4F (i4F) animals that displayed a tightly regulated temporal 4F gene expression of *Oct4*, *Sox2*, *KLF4*, and *c-MYC* in the heart upon doxycycline treatment (**Figure 3.3A**). Additionally, ACM-specific gene expression addressed a limitation of the global 4F gene expression model[6], which displayed lethality in mice with four consecutive days of expression. In our protocol, we allowed mice to reach adulthood, ensuring ACMs were terminally differentiated. Then we induced 4F gene expression for 2 straight weeks with doxycycline chow (**Figure 3.3B**). We confirmed the expression of *Oct4*, *Sox2*, and *c-Myc* in this model, up-regulated 18-fold and 16-fold, and 4-fold vs. control (-Dox), respectively, **P*<0.05 (**Figure 3.3C**).

We also determined elevated levels of 4F protein expression by immunofluorescence staining and immunoblotting in i4F animals compared to controls (**Figure 3.4A**). To assess a potential proliferative response, we evaluated gene expression levels of a panel of cardiac, cell cycle, and stemness genes. We observed a significant increase in the expression of late cell cycle genes *Ccnb1* and *AurkB*, 2.9-fold, and 3.4-fold, respectively, in i4F vs. control ACMs, *P<0.05 (**Figure 3.4B**). 4F expression yielded no significant difference in HW/BW in i4F mice compared to control mice (**Figure 3.4C**), or ACM cell size (data not shown).

To determine if the expression of 4F after terminal differentiation could promote robust CM proliferation and regenerative response in adults, we performed sham and MI surgeries in 10-week old mice. Analysis of cardiac function 14-days post-MI showed no significant differences in functional response to myocardial infarction in i4F mice vs. control (**Table 3.1**).

Our results demonstrate that our model could robustly express 3 of the 4 Yamanaka factors *Oct4*, *Sox2*, and *c-Myc*. Induction of these genes leads to an upregulation of late cell cycle genes although limited. However, there was no elevated expression of stemness genes, an indicator of dedifferentiation. We also do not see a significant difference in HW/BW after a two-week induction, nor improvement in cardiac functional post-MI in i4F mice compared to controls.

3.2.2 *ACM-specific 4F reprogramming factor constitutively active mouse model.*

After determining that our i4F mouse model could only express three of the four 4F genes, failing to induce KLF4, thought to be required for cellular reprogramming. We chose to mate our 4F-tet mouse with a CM-specific tetracycline-controlled transactivator (tTA) mouse. In this model, the presence of doxycycline reduces expression from the 4F tet-responder (**Figure 3.5A**). Induction of 4F was started from conception until adulthood, by feeding pregnant mothers and weaned pups normal (-Dox) chow (**Figure 3.5B**). At 8-10 weeks, we harvested hearts and isolated cardiac myocytes for downstream study. We again analyzed 4F gene expression, and like in the rtTA inducible model above, we saw an upregulation in only three of the four genes. *Oct4* (13-fold), *Sox2* (8-fold), and *c-Myc* (2-fold), *$P<0.05$, and no significant increase in *KLF4* gene expression (**Figure 3.5C**).

To determine whether the expression of these genes from conception through adulthood in ACMs could potentiate a pro-regenerative response, we evaluated gene expression levels of cardiac, cell cycle, and stemness genes. We saw an increase in the expression of late cell cycle genes *Cdk1* and *AurkB*, 2-fold, and 2.6-fold, respectively, in 4F vs. control ACMs. We also saw a 1.5-fold induction in the stemness gene *Dab2* (**Figure 3.6A**). *Dab2* has previously been reported as a marker of dedifferentiation in ACMs[5] and is a target of the cardiac transcription factors GATA4[9]. Nevertheless, constitutive 4F gene expression yielded no significant difference in HW/BW in 4F mice compared to control mice (**Figure 3.6B**) or ACM cell size (data not shown). However, we did observe an interesting phenotype in these mice. Males had bilateral testicular enlargement (**Figure 3.6C**), which presented by three weeks of age and persisted throughout the life of the mice. This observation was unexpected because 4F gene expression in this model is driven by a CM-specific alpha myosin heavy chain tTA promoter, which to date, expression of this cardiac gene has not been reported in the testes through fetal development.

3.3 DISCUSSION

In this chapter, we proposed a model to enhance the regenerative potential of ACMs, dedifferentiating them through partial reprogramming. We utilized the Yamanaka factors *Oct4*, *Sox2*, *Klf4*, and *c-Myc* (4F) in an attempt to reprogram ACMs *in vivo.* We ultimately tested this model by subjecting 4F expressing mice to an MI and determined the response of the CM. We generated two models, both ACM specific for 4F expression, one tet-on (inducible) and the other tet-off (constitutive).

Evaluation of 4F gene expression showed that both models were able to express *Oct4*, *Sox2*, and *c-Myc* robustly. However, there was no increase in gene expression of *KLF4* in our model. Our inability to induce *KLF4* gene expression hindered our study's capacity to assess the overexpression of all four factors in the ACM. KLF4 belongs to a family of zinc-finger transcription factors and is essential for reprogramming. However, its function depends on the gene targeted and can either activate or repress transcription depending on cellular contexts[10]. The expression of *KLF4* is seen in non-dividing terminally differentiated cells, playing an essential role in the regulation of homeostasis[10]. Yet, in iPSC generation, KLF4 directly binds to the promoter of Nanog to help *Oct4* and *Sox2* regulate *Nanog* expression. Therefore, *KLF4* expression present in terminally differentiated ACMs may be subverting their reprogramming potential.

With the overexpression of 4F, we did get a limited induction of cell cycle genes (~2-fold). Furthermore, there was no significant difference in HW/BW or ACM cell size after two-weeks of induction nor improvement in cardiac function post-MI. The lack of a robust cardiac phenotype may be attributed to numerous things. For one, our induction timeline may need to be

extended beyond two weeks. A lengthened timeline of four, six, or even eight weeks could allow for more time for the reprogramming factors to effect terminally differentiated ACMs.

Another possible limitation is that there may be a mosaic of 4F induction. If there is a mosaic of scattered 4F induction throughout the heart, analysis to determine the percentage of induced CM would be appropriate. Dedifferentiation of Oct4 positive CMs could be visualized by co-staining for Oct4, cell cycle activity (BrdU), and CM marker (PCM1). Single-cell RNA sequencing of Oct4 positive CMs could also determine any potential proliferative populations of CMs. Finally, terminally differentiated CMs may be especially resistant to reprogramming *in vivo*. If that is the case, a great deal of insight could still be gleaned from an *in vitro* study. One way to overcome the lack of *KLF4* expression in this model would be to culture 4F ACMs and transfect them with a KLF4 AAV virus along with dox induction or culture wild-type ACMs and transfect with 4F AAV virus. Studies like these would be an effective method to determine the molecular mechanism of reprogramming and changes to the epigenome of reprogrammed ACMs.

3.4 METHODS

Mouse Studies. All animal studies were performed in accordance with an approved Institutional Animal Care and Use Committee (IACUC protocol #4290-01), the University of Washington institutional guidelines, and the National Institute of Health Guide for the Care and Use of Laboratory Animals. The αMHC-tTA (tet-off) mice used for constitutive CM-specific transgene expression was generated by the Robbins lab[11]. The αMHC-rtTA (tet-on) mice used for inducible ACM-specific transgene expression was generated by the Valencik Lab[7]. Transactivator lines were crossed with the tet-responsive 4F mice[8] to generate the $4F^{Tg/+}$ model. For temporal control of transgene activity, we used doxycycline-containing chow (Harlan TD.00502) administered ad lib for the indicated times.

2-D Echocardiography. Under 0.5% isoflurane, mice EKG and heart function were assessed using Visual Sonics Vevo 2100. Parasternal short axis images at the plane of the papillary muscle were collected in B- and M-Modes. Images were collected with heart rates ranging from 400-500 BPMs. Imaging and analysis were performed by a single operator who was blinded to the genotypes. Quantification of images was performed using Vevo Labs 1.7.0, according to the manufacturer's guidelines.

CM cell isolation. We utilized established protocols for CM isolations[12,13]. Briefly, heparinized mice were euthanized with isoflurane and hearts were extracted and arrested in KB buffer (mmol/L: KCl 20, KH_2PO_4 10, K+-glutamate 70, $MgCl_2$ 1, glucose 25, taurine 20, EGTA 0.5, HEPES 10, 0.1% albumin, pH 7.4 with KOH). For purified ACM preparations, the aorta was cannulated, and the heart was washed with Tyrodes solution (pH 7.4, supplemented with 25uM Blebbistatin -/-) and digested for 7 minutes with collagenase II (Worthington 4176) and Protease Streptomyces griseus XIV (Sigma P5147) using Langendorf perfusion. Ventricles were

dissociated and the resulting cell suspension was filtered through a 100μm mesh. Three rounds of low speed centrifugation, where ACMs are loosely pelleted and non-CMs in suspension are aspirated, density purify the ACM population, resulting in >90% rod-shaped ACMs.

Immunoblotting. Immunoblotting was done as described previously[12,13]. CMs were lysed and whole cell lysates were separated on 12% gel, transferred onto PVDF membranes and probed with the following antibodies against: Oct4 (abcam19857).

RNA isolation and analysis. RNA was isolated from cells and tissue using TRISOL (Sigma T9424) phenol/chloroform purification, followed by column purification with DNase treatment (Qiagen 74004). cDNA was synthesized as described in the manufacturer's guidelines (Roche 04896866001). qPCR was performed using SYBR green (Life Technologies 4472908) on a real-time PCR machine (ABI 7900HT). Primers were validated by standard PCR with electrophoresis to confirm specific target band and lack of primer dimers. qPCR dissociation curves were consistent with a single specific product. Ct values were assigned using ABI's SDS 2.4 software with automated thresholding and baselines. The standard curve method or dCt method was used to quantify expression, and expression of each gene was normalized by *GAPDH*. Standard Curves were generated using tissue or cells that highly express the indicated gene, resulting in qPCR efficiencies ranging from 88-97%.

Histological studies. For histological analysis, hearts were fixed with 4% PFA. Paraffin sections were immunostained using standard protocol with Oct4 (Ab19857), WGA, (Life Technologies W6748), a marker for plasma membrane, and Hoechst (Life Technologies H3570) to visualize nuclei. Images were acquired with wide field microscopy (Nikon A1R).

3.5 FIGURES

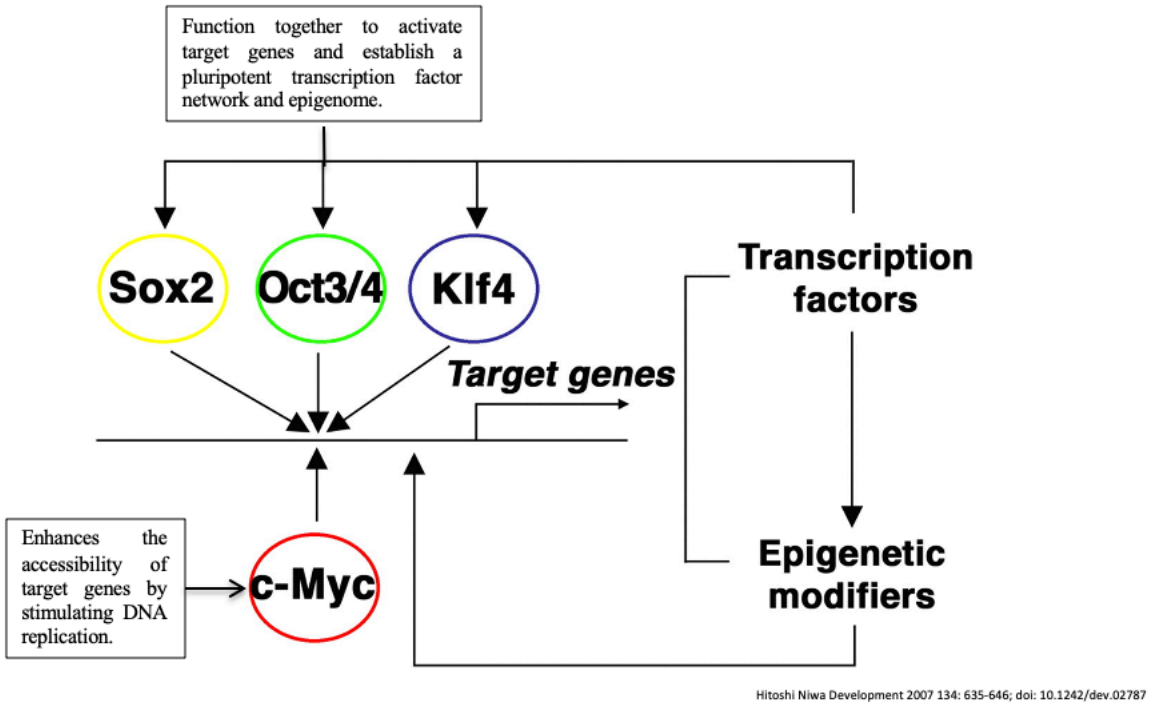

Figure 3.1: Schematic describing four Yamanaka transcription factors and their role in reprogramming differentiated cells into iPSCs.

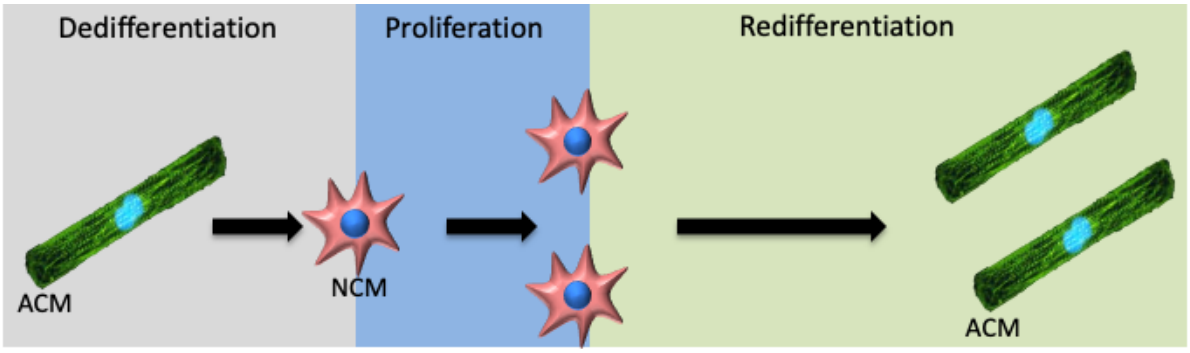

Figure 3.2: Schematic diagram for the process of mouse ACM dedifferentiation, proliferation and redifferentiation.

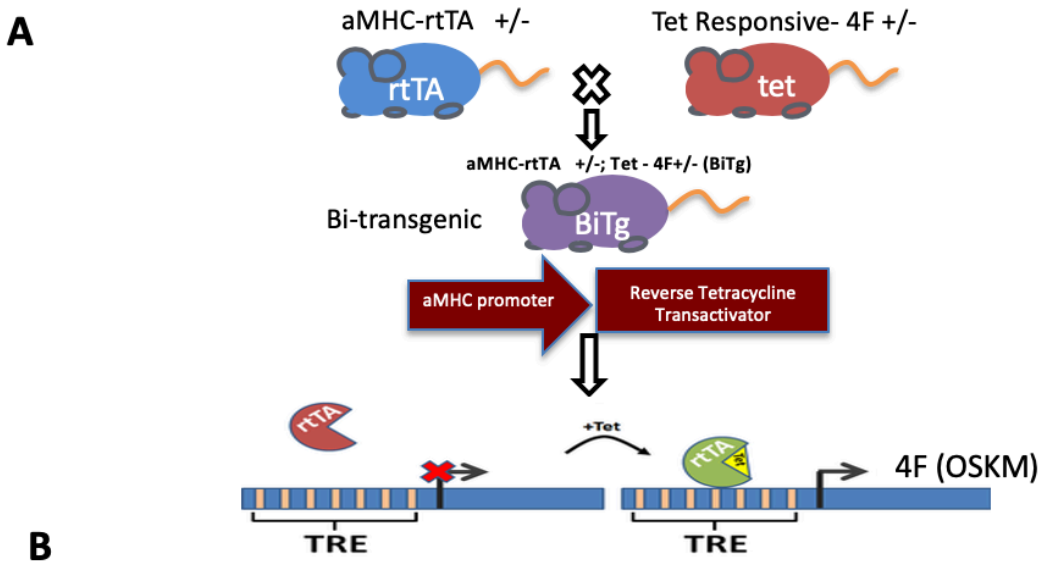
A
aMHC-rtTA +/-
Tet Responsive- 4F +/-
rtTA
tet
aMHC-rtTA +/-; Tet - 4F+/- (BiTg)
Bi-transgenic
BiTg
aMHC promoter
Reverse Tetracycline Transactivator
rtTA
+Tet
rtTA
4F (OSKM)
TRE
TRE

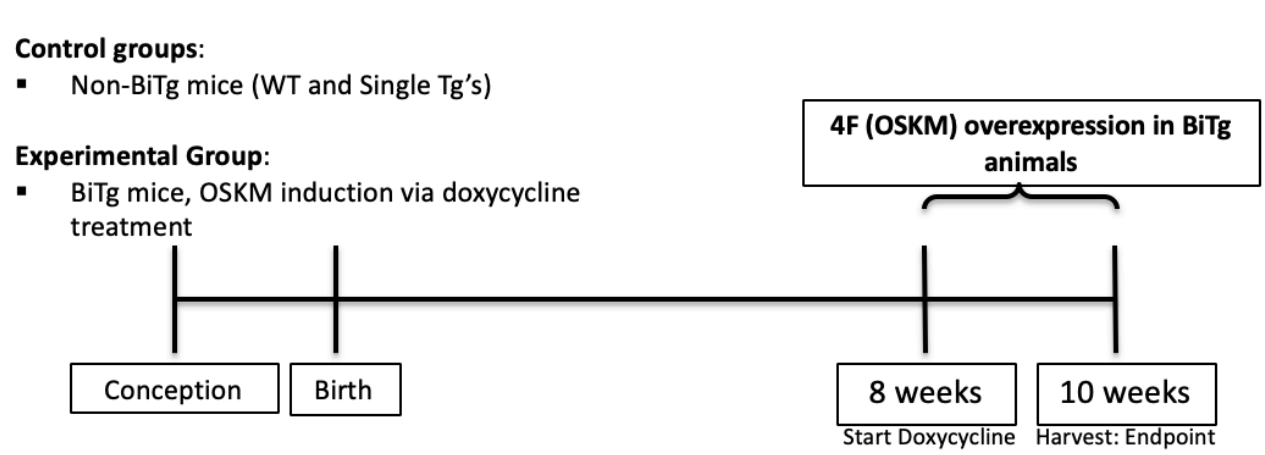
B
Control groups:
Non-BiTg mice (WT and Single Tg's)
Experimental Group:
BiTg mice, OSKM induction via doxycycline treatment
4F (OSKM) overexpression in BiTg animals
Conception
Birth
8 weeks
Start Doxycycline
10 weeks
Harvest: Endpoint


C
Fold Induction
25
20
15
10
5
0
*†‡
*†‡
*†‡
Oct4
Sox2
Klf4
cMYC
Control (-Dox)
Control (+Dox)
4F (-Dox)
4F (+Dox)

Figure 3.3: Inducible 4F mouse model construction, induction protocol, and 4F gene expression levels relative to GAPDH. (A) Schematic showing breeding strategy resulting in inducible 4F mice, and 4F(OSKM) induction in BiTg CMs. (B) Timeline showing protocol for ACM-specific 4F expression and endpoints. (C) 4F transgenes expression is robustly induced in inducible 4F ACMs fold induction vs. control (-Dox), expression normalized to *Gapdh. Sample Number:* (C) ≥ 3 animals per group. *Statistics:* Two-way ANOVA, * $P<0.05$ vs. ctrl (-Dox), † $P<0.05$ vs. ctrl (+Dox), ‡ $P<0.05$ vs. 4F (-Dox).

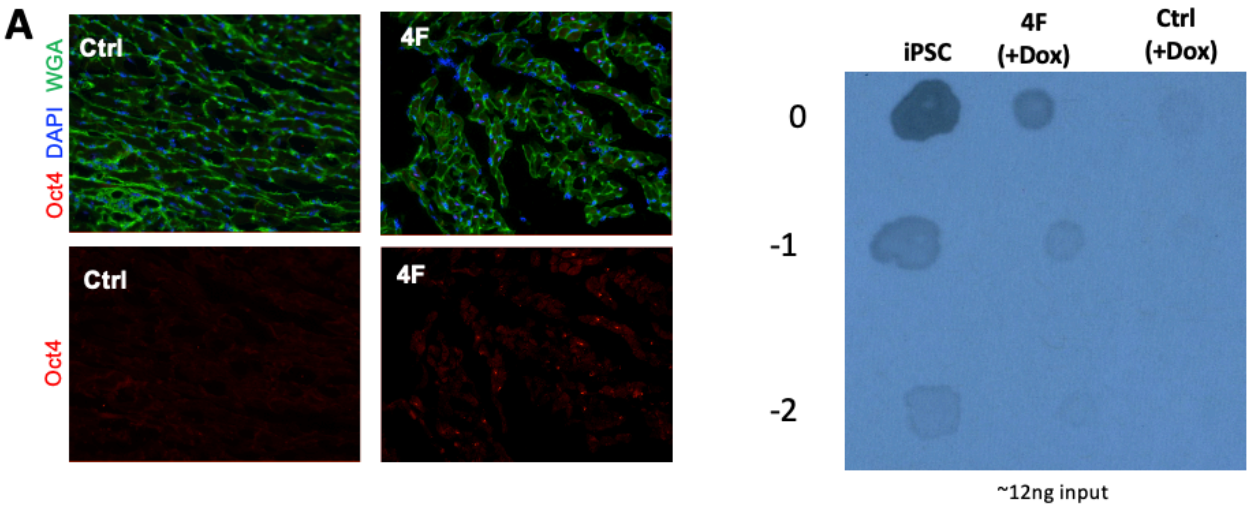
A
Oct4 DAPI WGA
Ctrl
4F
Oct4
Ctrl
4F
iPSC
4F (+Dox)
Ctrl (+Dox)
0
-1
-2
~12ng input

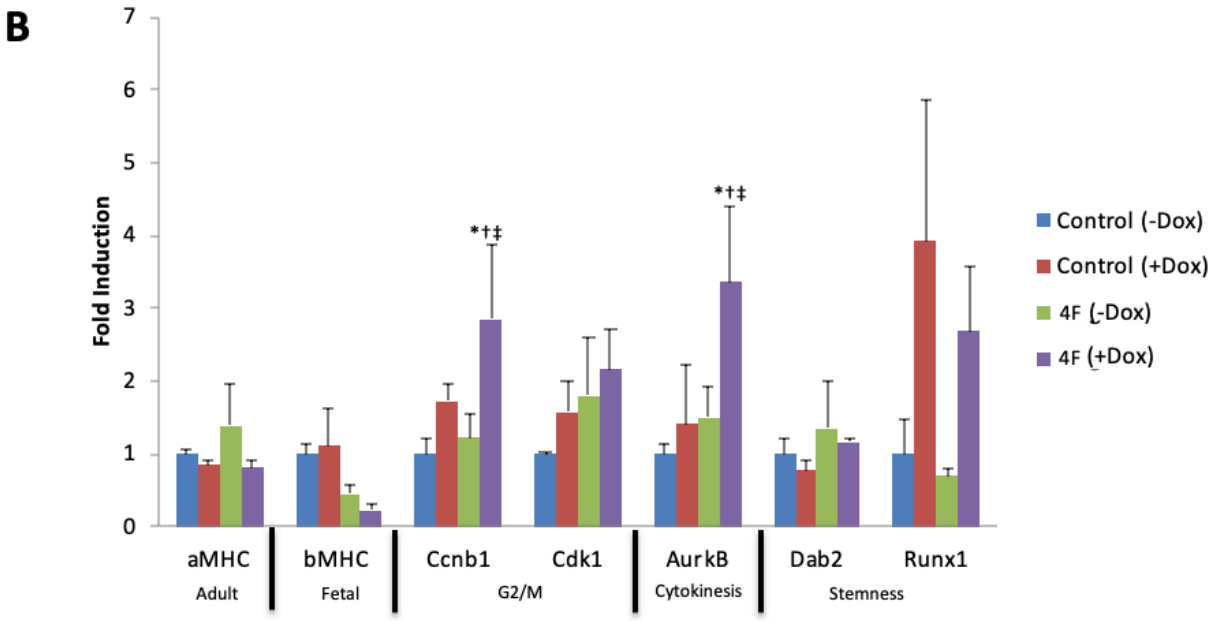
B
Fold Induction
0
1
2
3
4
5
6
7
*†‡
*†‡
aMHC
Adult
bMHC
Fetal
Ccnb1
Cdk1
G2/M
AurkB
Cytokinesis
Dab2
Runx1
Stemness
Control (-Dox)
Control (+Dox)
4F (-Dox)
4F (+Dox)

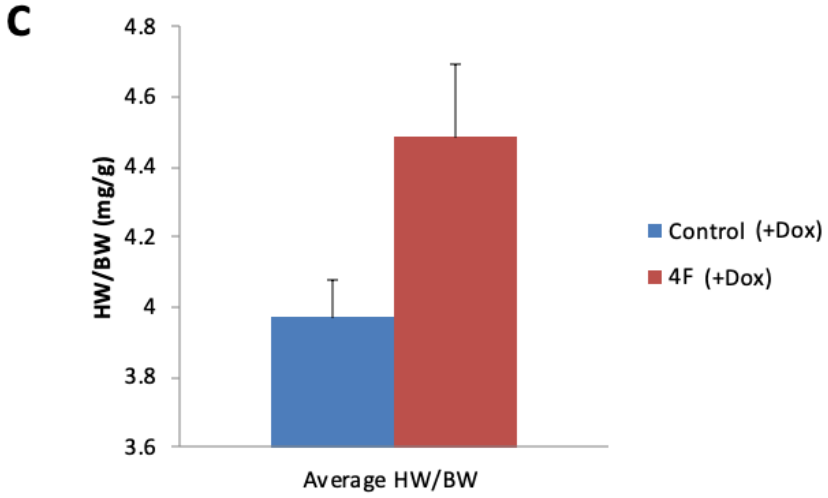
C
HW/BW (mg/g)
3.6
3.8
4
4.2
4.4
4.6
4.8
Average HW/BW
Control (+Dox)
4F (+Dox)

Figure 3.4: Characterization of 4F induction in ACMs. (A) Left, Immunofluorescence staining for Oct4 protein expression in ctrl (+Dox) and 4F (+Dox) cardiomyocytes at 2-week induction timepoint. Right, Immunoblotting of ACM lysates showing CM-specific Oct4 protein induction in 4F hearts and no induction of Oct4 with two weeks of induction in ACMs, iPSC cells used as positive control of Oct4 protein expression. (B) Expression of CM, cell cycle, and stemness genes in isolated ACMs measured by qRT-PCR, fold induction vs. control (-Dox), expression normalized to *Gapdh*. (C) HW/BW quantification control (+Dox) and 4F (+Dox) mice. Sample Number: ((B) ≥3 animals per group (C) Control (+Dox) = 3, 4F (+Dox) = 3 Statistics: (B) Two-way ANOVA, *P < 0.05 vs ctrl (Dox), †P < 0.05 vs 4F (-Dox), ‡P < 0.05 vs ctrl (+Dox). (C) Two-tailed t-test, control (+Dox) vs 4F (+Dox), P > 0.05.

A

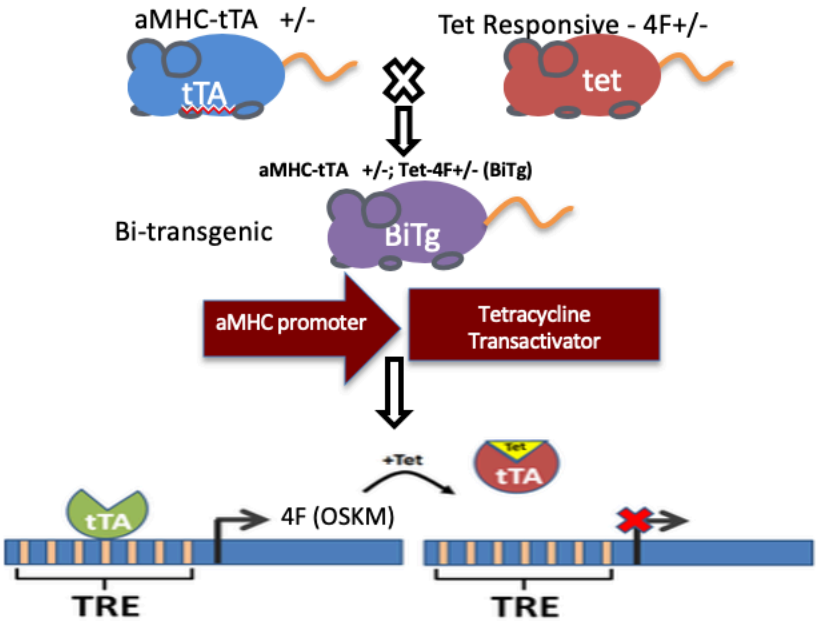

B

Control groups:

- Non-BiTg mice (WT and Single Tg's)

Experimental Group:

- BiTg mice, 4F activation in the absence of Dox

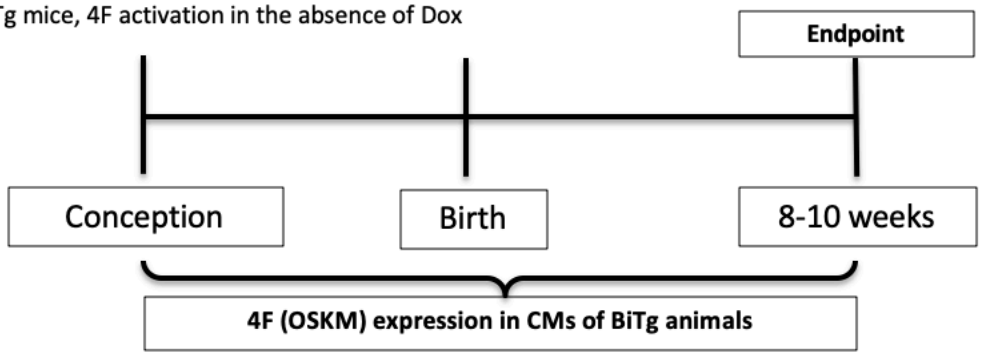

C

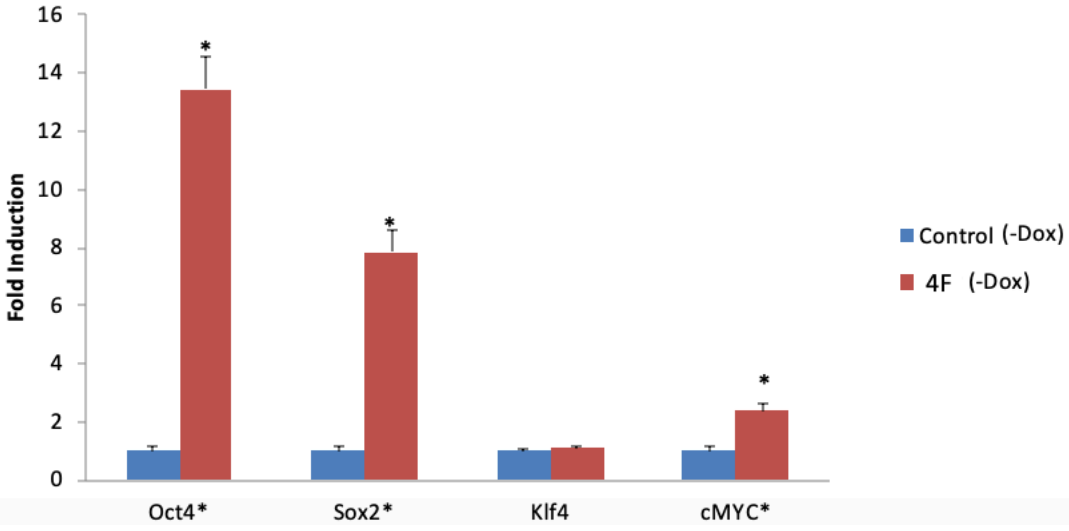

Figure 3.5: Constitutively expressed 4F mouse model construction, induction protocol, and 4F gene expression levels relative to GAPDH. (A) Schematic showing breeding strategy resulting in inducible 4F mice, and 4F (OSKM) constitutive BiTg CMs. (B) Timeline showing protocol for ACM-specific 4F expression and endpoints. (C) 4F transgenes expression is robustly induced in constitutively 4F expressing ACMs fold induction vs. control (-Dox), expression normalized to *Gapdh. Sample Number:* (C) ≥ 3 animals per group. *Statistics:* T-test, * $P<0.05$ vs. ctrl (-Dox).

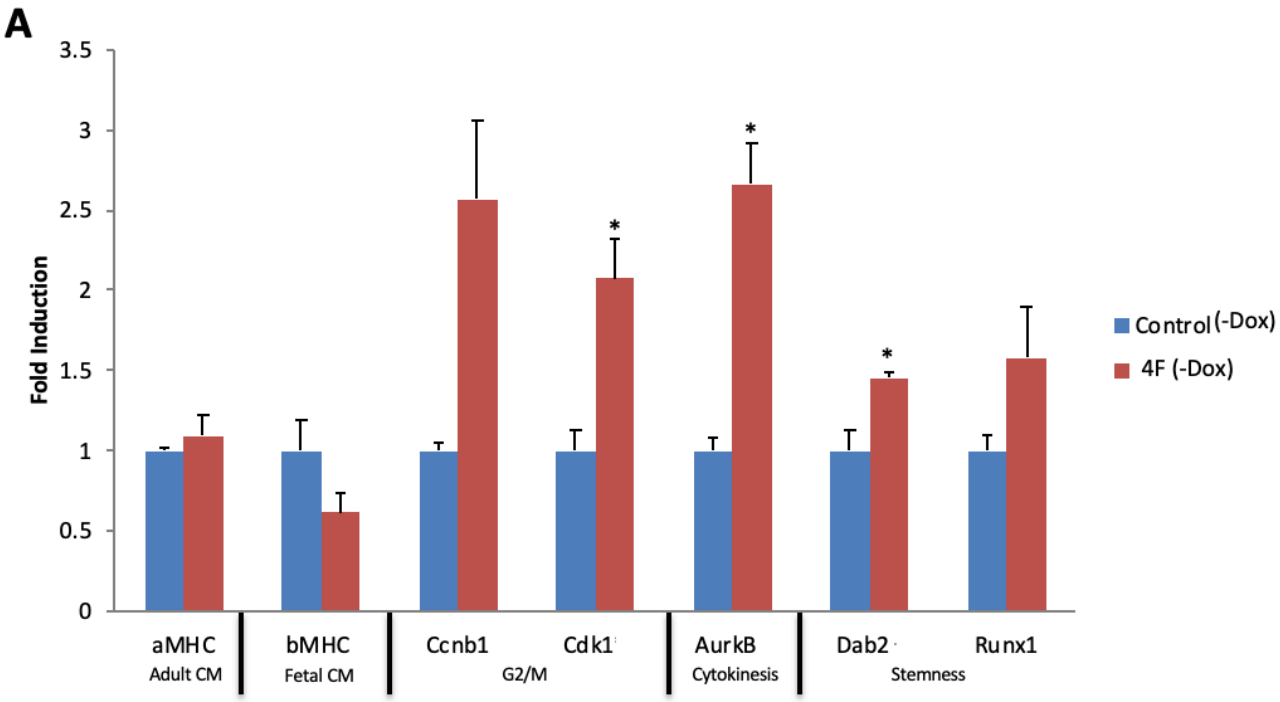
A
Fold Induction
3.5
3
2.5
2
1.5
1
0.5
0
*
*
*
aMHC
Adult CM
bMHC
Fetal CM
Ccnb1
Cdk1
G2/M
AurkB
Cytokinesis
Dab2
Runx1
Stemness
Control (-Dox)
4F (-Dox)

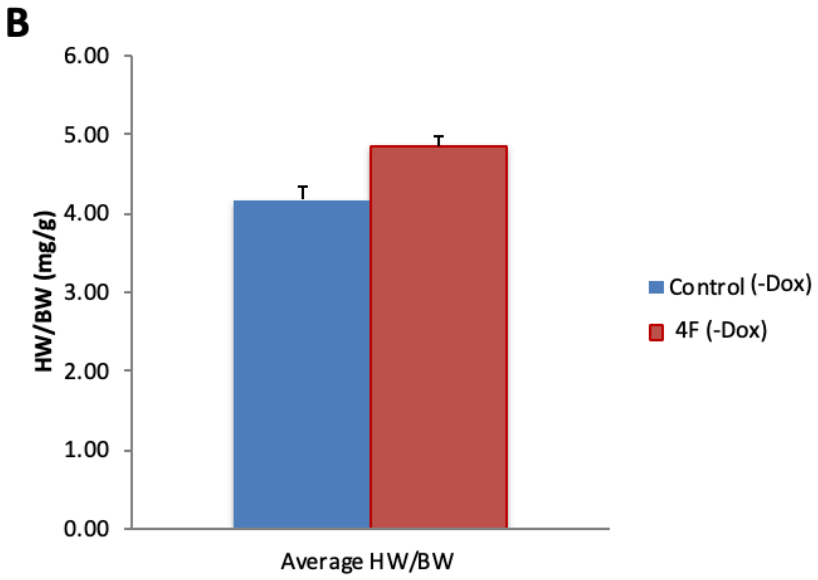
B
HW/BW (mg/g)
6.00
5.00
4.00
3.00
2.00
1.00
0.00
Average HW/BW
Control (-Dox)
4F (-Dox)

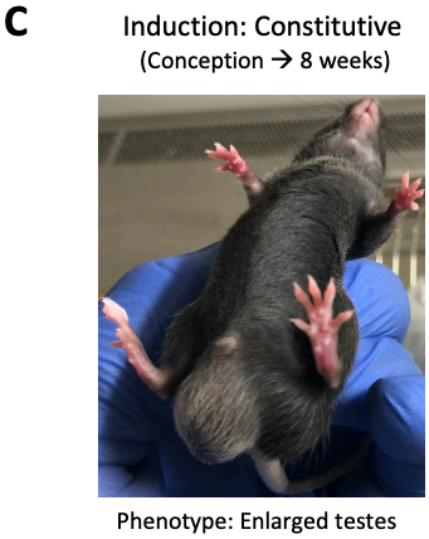
C
Induction: Constitutive
(Conception → 8 weeks)
Phenotype: Enlarged testes

Figure 3.6: Characterization of constitutively expressing 4F mice. (A) Expression of CM, cell cycle, and stemness genes in isolated ACMs measured by qRT-PCR, fold induction vs. control (-Dox), expression normalized to *Gapdh*. (B) HW/BW quantification control (-Dox) vs. 4F (-Dox) mice. (C) Image of 8-week-old male 4F mouse with constitutive expressions for 4F(OSKM) genes, showed significant increase in testicular size compared to control (not shown) which had normal testes phenotype. *Sample Number*: (B) ≥3 animals per group (C) Control (-Dox) = 3, 4F (-Dox) = 3 *Statistics*: (A-B) Two-tailed t-test, $P > 0.05$ vs ctrl (-Dox)

3.6 TABLE

Table 3.1. Cardiac function and morphology in 4F MI-operated mice. Echocardiography results in 12-week old mice, 14 days post-operation. HR: Heart Rate, EF: Ejection Fraction, FS: Fractional Shorting, CO: Cardiac Output, LVEDD: Left Ventricular End-Diastolic Dimension. Mean, and SEM values are shown. *Sample Number:* Sham, Control=4, 4F=4; MI, Control=3, 4F=5. *Statistics:* Two-way ANOVA/Tukey's test, control vs. 4F, $P > 0.05$.

	Control		4F	
	Sham	MI	Sham	MI
HR (BPM)	596.95 ± 3.23	523.58 ± 99.48	547.73 ± 27.64	526.04 ± 38.07
EF (%)	93.4 ± 4.59	45.33 ± 1.56	88.58 ± 3.53	41.15 ± 3.48
FS (%)	67.68 ± 8.84	21.57 ± 1.22	57.91 ± 5.08	19.81 ± 2
CO (mL/min)	27.96 ± 2.17	8.16 ± 5.67	16.57 ± 3.12	14.85 ± 5.67
LVEDD (mm)	3.48 ± 0.18	2.86 ± 0.55	2.86 ± 0.55	3.90 ± 0.53

3.7 BIBLIOGRAPHY – CHAPTER 3

1. Benjamin EJ, Virani SS, et al. Heart Disease and Stroke Statistics-2018 Update: A Report From the American Heart Association. Circulation. 2018 Jan 31

2. Ahuja P, Sdek P, MacLellan WR. Cardiac myocyte cell cycle control in development, disease, and regeneration. Physiol Rev 2007 87(2):521-44.

3. Takahashi, K., Yamanaka, S. (2006). Induction of pluripotent stem cells from mouse embryonic and adult fibroblast cultures by defined factors. Cell 126:663-676.

4. Zhang, Yiqiang et al. "Dedifferentiation and proliferation of mammalian cardiomyocytes." PloSone vol.5,9e12559.3

5. Wang, Wei Eric et al. "Dedifferentiation, Proliferation, and Redifferentiation of Adult Mammalian Cardiomyocytes After Ischemic Injury." Circulation vol. 136,9 (2017): 834-848.

6. Ocampo A, Reddy P, Izpisua Belmonte JC. In Vivo Amelioration of Age-Associated Hallmarks by Partial Reprogramming. Cell Volume 167, Issue 7, 15 December 2016, Pages 1719–1733.e12.

7. Valencik ML, McDonald JA. Codon optimization markedly improves doxycycline-regulated gene expression in the mouse heart. Transgenic Res. 2001 Jun;10(3):269-75.

8. Carey, B.W., Markoulaki, S., Beard, C., Hanna, J., and Jaenisch, R. (2010). Single-gene transgenic mouse strains for reprogramming adult somatic cells. Nat. Methods 7, 56–59.

9. Kubin T, Pöling J, Kostin S, Gajawada P, Hein S, Rees W, Wietelmann A, Tanaka M, Lörchner H, Schimanski S, et al. Oncostatin M is a major mediator of cardiomyocyte dedifferentiation and remodeling. Cell Stem Cell. 2011; 9:420–432.

10. Katz, Jonathan P et al. “The zinc-finger transcription factor Klf4 is required for terminal differentiation of goblet cells in the colon.” Development (Cambridge, England) vol. 129,11 (2002): 2619-28.

11. Sanbe, A. *et al.* Reengineering Inducible Cardiac-Specific Transgenesis With an Attenuated Myosin Heavy Chain Promoter. *Circ. Res.* 92**,** 609–616 (2003).

12. Sdek, P. *et al.* Rb and p130 control cell cycle gene silencing to maintain the postmitotic phenotype in cardiac myocytes. *J. Cell Biol.* 194, 407–23 (2011).

13. El-Nachef, D. *et al.* Repressive histone methylation regulates cardiac myocyte cell cycle exit. *J. Mol. Cell. Cardiol.* 121, 1–12 (2018).

VITA

Miles Freeman was born in Orlando, Florida. He attended Florida State University where he completed a bachelor's degree in Biological Sciences in 2011. Afterward, he completed his master's thesis project in the department of pharmaceutical science at Florida Agricultural & Mechanical University. Following the completion of his master's degree, he began studying medicine at Morehouse School of Medicine in Atlanta, Georgia, before being recruited to participate in the Morehouse School of Medicine-University of Washington Allied Medical Scientist Training Program. In 2016, he joined the Molecular and Cellular Biology graduate program. He began his thesis work in Robb MacLellan's lab at the University of Washington South Lake Union campus. Miles received his Doctor of Philosophy in 2020 and returned to Morehouse School of Medicine to complete his medical training.